UNIVERSITY OF CALIFORNIA,
IRVINE

NANOTUBE INTERACTIONS WITH NANOPARTICLES AND PEPTIDES

DISSERTATION

submitted in partial satisfaction of the requirements
for the degree of

DOCTOR OF PHILOSOPHY

in Electrical and Computer Engineering

by

Lifeng Zheng

Dissertation Committee:
Professor Peter Burke, Chair
Professor Chin Lee
Professor Zhongping Chen

2008

The dissertation of Lifeng Zheng
is approved and is acceptable in quality and form
for publication on microfilm and in digital formats:

Committee Chair

University of California, Irvine
2008

TABLE OF CONTENTS

LIST OF FIGURES

LIST OF TABLES

ACKNOWLEDGEMENTS

“Research in this field is just like surfing. If you don’t stand on the top of the wave, you can not catch it up any more.” I was deeply touched by this sentence when Professor Peter Burke, my advisor, told me about the exciting side of nanotechnology in the first year of my PhD study. And in the following years, I have been trying hard to catch up the wave. Also, as a great mentor, Peter has always been my role model showing how to approach and tackle a scientific problem while enjoying the process. Today, I would like to express my most sincere appreciation and deepest gratitude to Peter for his great guidance, persistent help, and financial support which made this dissertation possible.

I would like to thank my lab mates. I could not have finished this thesis without their help and discussion. They are Sheldon Shengdong Li, Jenny Zhen Yu, Sungmu Kang, Chris Rutherglen and Dheeraj Jain. I have also enjoyed the technical discussions with Weiwei Zhou on the growth and characterization of carbon nanotubes.

I would also like to thank Professor Jim Brody for the collaboration, his assistant Joe for the instructions on bioexperiments, Kirsty Salmon in the lab of ORU Genomics & Bioinformatics for the help on DNA synthesis and Juan Diaz in Weiss Lab for the instructions in phage display experiments.

This work was supported by the U.S. National Science Foundation, the Army Research Office, the Office of the Naval Research, DARPA and the Keck Foundation.

CURRICULUM VITAE

Lifeng Zheng

EDUCATION

Ph.D. Electrical and Computer Engineering — 2008
University of California, Irvine — *Irvine, California*

M.S. Electrical Engineering — 2000
Old Dominion University — *Norfolk, Virginia*

M.S. Astrophysics — 1997
Beijing University — *Beijing, China*

B.E. Precise Instruments and Control — 1992
Nanjing University of Aeronautics and Astronautics, China — *Nanjing, China*

RESEARCH EXPERIENCE

Graduate research assistant — 2002-2008
University of California, Irvine — *Irvine, California*

Graduate research assistant — 1997-2000
Old Dominion University — *Norfolk, Virginia*

Graduate research assistant — 1994-1997
Beijing University — *Beijing, China*

INDUSTRY EXPERIENCE

Java programmer — 2000-2001
Data Direct Networks, Inc. — *Monrovia, California*

Gyroscope architect — 1992-1994
Shanghai Astronautics 803 Institution — *Shanghai, China*

JOURNAL PUBLICATIONS

L. Zheng, D. Jain and P.J. Burke, "Probing nanotube-protein interactions on a

silicon chip using molecular biology tools", *Small*, in process.

A.Y. Chen, A.S. Jani, **L. Zheng**, P.J. Burke and J.P. Brody, "Microfabricated Arrays of Cylindrical Wells Facilitate Single-Molecule Enzymology of α-Chymotrypsin" *Biotechnology Progress*, in process.

L. Zheng, S. Li, J.P. Brody, P.J. Burke, "Manipulating nanoparticles in solution with electrically contacted nanotubes using dielectrophoresis", *Langmuir,* 20, 8612, 2004.

L. Zheng, J.P. Brody, P.J. Burke, "Electronic Manipulation of DNA, Proteins, and Nanoparticles for Potential Circuit Assembly" *Biosensors & Bioelectronics,* **20**, 606, 2004.

L. Zheng, R.P. Joshi and C. Fazi, "Effects of barrier height fluctuations and electron tunneling on the reverse characteristics of 6H-SiC Schottky contacts", *Journal of Applied Physics*, **85**, 3701, 1999.

L. Zheng, R.P. Joshi and C. Fazi, "Dislocation defect based model analysis for the prebreakdown reverse characteristics of 4H-SiC p+n diodes", *Journal of Applied Physics*, **85**, 7935, 1999.

Wu YF, Li YX and **Zheng LF,** "A search for high-velocity gas in massive star formation regions", *Chinese Astronomy and Astrophysics*, **22**, 459, 1998.

CONFERENCE PUBLICATIONS

L. Zheng, P. J. Burke, and J. P. Brody, "Electronic manipulation of DNA and proteins for potential nano-bio circuit assembly" *Proc. of SPIE* **5331**, 126, 2004.

L. Zheng, S. Li and P. J. Burke, "Self-Assembled Gold Nanowires from Nanoparticles: An Electronic Route Towards DNA Nanosensors", *Proc. of SPIE, Photonics West, Bios 2004* (2004), San Jose, CA.

L. Zheng, S. Li, P.J. Burke, J.P. Brody, "Towards Single Molecule Manipulation with Dielectrophoresis Using Nanoelectrodes", *Proceedings of the 3rd IEEE Conference on Nanotechnology*, **1**, 437, 2003.

ABSTRACT OF THE DISSERTATION

Nanotube Interactions with Nanoparticles and Peptides

by

Lifeng Zheng

Doctor of Philosophy in Electrical and Computer Engineering

University of California, Irvine, 2008

Professor Peter Burke, Chair

Understanding of interactions between single-walled carbon nanotubes and other materials is critical for developing a new technology of self-assembling carbon nanotubes into electronics or drug delivery systems. We demonstrate for the first time the use of nanotube electrodes to manipulate nanoparticles in solution using dielectrophoresis. On the other hand, to understand a non-electrical assisted interaction, we investigate the binding affinity of carbon nanotubes and peptides via combinatorial phage display technique. We find a tryptophan rich binding motif to nanotubes on solid silicon substrates. The motif resembles an alpha helix with tryptophan concentrated along one side that binds non-covalently via π-π interactions to the walls of the nanotube.

CHAPTER 1

INTRODUCTION

It is fair to say that it was after Iijima published his work[1] in 1991 did Carbon nanotubes draw considerable attention, although they were first discovered in 1952 by Russian scientists[2] and nantoubes were then called “carbon tubules”. Carbon nanotubes have given rise to tremendous interest due to their unique mechanical and electronic properties, such as extremely high strength, elasticity, thermal conductivity, aspect ratio and unique electronic properties[3]. They are extremely promising for the applications in scanning probes, field emission devices, electronics devices, photonic detectors, armour reinforcement, chemical sensors, biosensors, drug discovery and delivery systems.

1.1 Geometric structures

Carbon nanotube are one of the many forms in which carbon is found in nature, which can be seen as a layer of graphite rolled up into a seamless cylinder with a diameter of a few nanometers as shown in Figure 1. The roll-up vector $\vec{C}_h$ known as the chiral vector, which determines the circumference of the nanotube, can be describe with two unit vectors $\vec{a}_1$ and $\vec{a}_2$ as

$$\vec{C}_h = n\vec{a}_1 + m\vec{a}_2 .$$

These two unique vectors $\vec{a}_1$ and $\vec{a}_2$ in the Cartesian coordinate system are expressed as

$$\vec{a}_{1,2} = \left(\frac{\sqrt{3}}{2}a, \pm a\right),$$

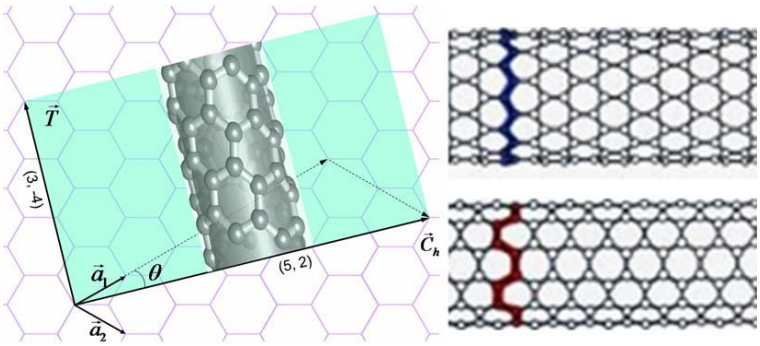

Figure 1.1. A graphite rolled up into a (5,2) nanotube. Depending on the roll-up vector, a carbon nanotube can be zigzag, armchair or chiral.

where a is the length of the unit vector, given by

$$a = |\vec{a}_{1,2}| = \sqrt{3} \times 1.42\ \dot{A} = 2.46\ \dot{A}$$

Then the diameter of the nanotube d_t, which can be calculated from $\vec{C}_h$, and the the chiral angle θ , are expressed in terms of the chirality index (n,m) in the following way:

$$d_t = \frac{|\vec{C}_h|}{\pi} = \frac{a}{\pi}\sqrt{n^2 + nm + m^2}$$

and

$$\theta = \tan\left(\frac{\sqrt{3}m}{2n + m}\right)$$

We denote (n,n) tube armchair nanotube ($\theta = 30^\circ$) and (n,0) one ($\theta = 0^\circ$) zigzag tube. If the angle is other than these two degrees, the tube is called chiral nanotube.

The chirality index also determines the translational lattice vector $\vec{T}$ which defines the length along the nanotube unit cell as

$$\vec{T} = t_1\vec{a}_1 + t_2\vec{a}_2$$

Since , t_1 and t_2 can be calculated as

$$t_1 = \frac{2m + n}{N_R}$$

and

$$t_2 = \frac{2n + m}{N_R}$$

where N_R is the greatest common divisor of $2m + n$ and $2n + m$.

The nanotubes described above are known as the single walled nanotubes (SWNTs) since the graphite sheet is rolled up into one layer. The smallest SWNTs reported so far are about 0.4 nm but usually less than 3 nm in diameter, although 5-nm SWNTs have also been reported. There are also multi-wall nanotubes (MWNTs) produced during the growth, depending on the catalysts used and the growth temperatures. The smallest MWNTs are the double-wall nanotubes (DWNTs) and the largest diameter of MWNTs can be over 100 nm.

1.2 Properties and applications

Similar to graphite, the neighboring atoms of carbon nanotubes forms strong sp^2 bonds or *σ bonds*, which are even stronger than the sp^3 bonds in dimond. On the per-bond basis, the sp^2 bond is one-third stronger than the sp^3 bond. This explains the unique strength of carbon naotubes. Carbon nanotubes are known so far to have the highest Young's modulus, over 1 TPa, which is 5 times as much as that of steel. Plus their hollow structures, carbon nanotubes are considered as the only candidate to make a space

elevator. No other materials can sustain the self-gravity when an elevator reaches the space. The thermal conductivity of carbon nanotubes along their axis is superior to that of other materials, even including diamond. Nanotubes can also sustain extremely high temperature with a melting point of about 4000 K, similar to that of graphite. These advantages can be derived from the strength of the sp^2 bond.

On the other hand, the electronic properties of carbon nanotubes are benefited from the π band. There are two types of single wall carbon nanotubes: metallic and semiconducting depending on their helix structures. Only those (n,m) nanotubes that satisfy $n-m$ is a multiple of 3 are metallic. The others are semiconducting. Hence, the armchair nanotubes are always conducting while one third of zigzag nanotubes are metallic and two thirds are semiconducting.

In the past decade, studies have proposed indicating potential applications of carbon nanotubes. Nanotube have been used as SPM tips and AFM probes for their high aspect ratios and excellent mechanical properties; metallic nanotubes have also been used in the field emission display systems since electrons are easily emitted from the nanotube tips under the low bias; semiconducting nanotubes have been applied in transistors and sensors; nanotubes are also used in killing cancer cells due to their infrared band gaps; nanotubes are an excellent candidate to store hydrogen due to the expandable sp^2 bond; as a substitute of ITO, nanotubes can act as transparent thin film in solar cells. Other applications of nanotubes can be in armour reinforcement, THz RF electronics, sports equipment, and so on.

1.3 Challenges and methods

However, even with the tremendous advances in the various applications due to their unique structures and properties, carbon nanotubes faces challenges in commercialization.

High temperature environment required for growth and hard control of growth direction make it difficult to be directly used after growth. The unwanted carbon soot or amorphous carbon generated during the growth and the metal catalysts should be removed prior to their uses in any products.

An ideal method to overcome these problems is the dispersion of carbon nanotubes in solutions. However, the inert properties of carbon nanotubes in chemistry and insolubility in aqueous solution are the issues to be concerned. Carbon nanotubes usually form nanotube bundles due to their super hydrophobicity and cause poor solubility and dispersion in the aqueous solution.

Functionalization of carbon nanotubes once has been a hot topic to solve the problem. However, functionalization of carbon nanotubes usually involves modifying the CNT surfaces in strong acidic solutions and destroys the pristine structures and thus the intrinsic electronic structures of nanotubes. Many defects may also be caused on carbon nanotubes by this method, and thus their excellent mechnical properties are not conserved.

Several methods have been developed to suspend carbon nanotubes in liquid solutions while avoiding the surface moidification. Basically, there are two kinds of liquid solutions (aqueous and organic solutions) to disperse carbon nanotubes.

For the aqueous solutions, surfactants, biomolecules and polymers are good materials. Surfactants are composed of water-soluble surface-active agents and a hydrophobic

portion, usually a long alkyl chain. Thanks of these structures, surfactants possess a common property of lowering the surface tension and thus are good candidates for dispersing carbon nanotubes in the aqueous solution.

Sodium dodecyl sulfate (SDS) was the first surfactant used to suspend carbon nanotubes in order to purify nanotubes among nanoparticles[4]. In that research, it was demonstrated that the dispersion of nanotubes reaches optimum in water when the SDS concentration slightly above the critical mecellar concentration (CMC, 2.5g/L). Either lower (0.4 CMC) or higher (12 CMC) causes aggregation and sedimentation. Another surfactant is benzalkonium chloride. Smalley's group used 0.1% benzalkonium chloride in aqueous solution to disperse CNTs[5].

However, the purification methods mentioned in the above publications need a number of successive filtration steps. Roth's group in Germany developed a recipe to achieve high-purity and size-selected nanotubes without filtration[6]: sonicate the nanotube suspension in 1 wt % (4 CMC) SDS aqueous solution for 2 minutes followed by chromatographic separation and centrifugation sediment.

SDS is the most frequently used anionic surfactant to disperse the carbon nanotubes in aqueous solutions for the research purposes such as SWNT chirality assignment with fluorescence spectroscopy[7-11], SWNT film printing[12] and charge transfer of SWNT arrays[13].

Besides SDS, other anionic surfactants, such as dodecyl-benzene sodium sulfonate (NaDDBS)[14,15], sodium cholate[16,17], sodium deoxycholate[17] and sodium taurodeoxycholate[17], nonionic surfactants, such as Triton-x 100[18], tween-80[19], and cationic surfactants, such as octadecyltrimethylammonium bromide (OTAB)[20], are all

used in dispersing SWNTs in aqueous solutions. Tween-20, which is used in our phage display experiments, also shows its good ability of dispersing carbon nanotubes.

Biomolecules have recently been given attention due to their abilities reducing the surface tension. Gum Arabic[21], a natural molecule complex of saccharides and glycoproteins, single-stranded DNA[22,23], phospholipids[24], have been shown to disperse carbon nanotubes well.

SWNT can also be solubilized in water by non-covalently functionalization with certain polymers: polyvinyl pyrrolidone (PVP)[25] and polystyrene sulfonate (PSS)[25] and fluorescein-PEG[26].

There are several organic solvents known to disperse single walled carbon nanotubes: dimethylformamide (DMF)[27], dichloroethane (DCE)[28], N-methylpyrrolidone[29], hexamethylphosphoramide[29], cyclopentanone[29], tetramethylene sulfoxide[29], and ε-caprolactone[29].

However, there are always some disadvantages of these methods in nanotube dispersion. Two major problems should be concerned. One is the concentration of nanotubes in solution. So far, there are only a small amount of nanotubes that can be dispersed in solutions. Another one is the stability of nanotube solutions. In most of these methods, nanotube solutions can not be stored over a month or even a couple of weeks. Nanotubes get bundled and precipitate at the bottom of the solutions.

1.4 Our thoughts

Our early investigation of carbon nanotube applications was focused on the manipulation of nanoparticles and biomolecules using carbon nanotubes as electrodes. The advantage

of using carbon nanotubes is nanotubes are so small in diameter so that they can generate very large electric fields near the tips and along the axis. A dielectrophoresis technique is used in the investigations. We will introduce this method in chapter 2. In the later chapters (chapter 3 and 4), we prove that dielectrophoresis is a successful tool in massive manipulations of nanoparticles and biomolecules.

In order to better solve the problems in nanotube dispersions and for carbon nanotube to be further used in other applicaitons, we think the first step is to understand how the nanotubes interact with other materials. Hence, an appropriate technique is used to tackle the problem – phage display. We also introduce it in chapter 2 and explore it in chapter 5. We found the motif of peptides that bind to nanotubes. This tells us the properties of interactions between nanotubes and peptides.

References

1. Iijima, S., *Nature* 354, 56–58, 1991.
2. Monthioux, M. and Kuznetsov V., *CARBON* 44, 1621, 2006.
3. Saito R., Dresselhaus G. and Dresselhaus M., Physical Properties of Carbon Nanotubes, Imperial College Press, 1998.
4. Bonard J, Stora T, Salvetat J, Maier F, Stockli T, Duschl C, Fod L, de Heer W, and Chbtelain A, *Adv. Muter*. 9, 827, 1991.
5. Bandow S, Rao A, Williams K, Thess A, Smalley R and Eklund P, J. *Phys. Chem. B* 101, 8839, 1997.
6. Duesberg G, Muster J, Krsti V, Burghard M and Roth S, *Appl. Phys. A* 67, 117, 1998.
7. Michael J. O'Connell, et al., *Science* 297, 593, 2002.
8. Sergei M. Bachilo, et al, *Science* 298, 2361, 2002.
9. Strano M, *J. Am. Chem. Soc.* 125, 16148, 2003.
10. Miyauchi Y., Chiashi S., Murakami Y., Hayashida Y., Maruyama S., *Chem. Phys. Lett.* 387, 198, 2004.
11. Weisman R., Bachilo S., Tsyboulski D., *Appl. Phys.* A 78, 1111, 2004.
12. Neitl M., Zhou Y., et al, *Nano Lett.* 4, 1643, 2004.
13. Lee C., Baik S., et al, *J. Phys. Chem. B* 110, 11055, 2006.

14. Islam M, Rojas E, Bergey D, Johnson A, Yodh A., *Nano Lett.* 3, 269, 2003.

15. Matarredona O, Rhoads H, Li Z, Harwell JH, Balzano L, Resasco D., *J Phys Chem B* 107, 13357, 2003.

16. Heller, D, Mayrhofer, R, Baik, S, Grinkova, Y, Usrey, M and Strano, M, *J. Am. Chem. Soc.* 126, 14567, 2004.

17. Michael S. Arnold, Alexander A. Green, James F. Hulvat, Samuel I. Stupp and Mark C. Hersam, *Nat. Nano.* 1, 60, 2006.

18. Nagahara L, Amlani I, Lewenstein J and Tsui R, *Appl. Phys. Lett.* 80, 3826, 2002

19. Lebedkin S, Hennrich F, Skipa T and Kappes M, *J. Phys. Chem. B*, 107, 1949, 2003.

20. Richard C, Balavoine F, Schultz P, Ebbesen T, Charles Mioskowski, *Science* 300, 775, 2003.

21. Bandyopadhyaya R, Nativ-Roth E, Regev O and Yerushalmi-Rozen R, *Nano. Lett.* 2, 25, 2002.

22. Zheng M, Jagota A, Strano M, Santos A, Barone P, Chou G, Diner B, Dresselhaus M, Mclean R, Onoa B, Samsonidze G, Semke E, Usrey M and Walls D, *Science* 302, 1545, 2003.

23. Zheng M, Jagota A, Semke E, Diner B, Mclean R, Lustig S, Richardson R and Tassi N, *Nat. Mat.* 2, 338, 2003.

24. Wu Y, Hudson J, Lu Q, Moore J, Mount A, Rao A, Alexov E and Ke P, J. Phys. Chem. B 110, 2475, 2006.

25. O'Connell M, Boul P, Ericson L, Huffman C, Wang Y, Haroz E, Kuper C, Tour J, Ausman K and Smalley R, *Chem. Phys. Lett.* 342, 265, 2001.

26. Nozomi N, Bangsaruntip S, Sun X, Welsher K and Dai H. *J. Am. Chem. Soc.* 129, 2448, 2007.

27. Liu J, Casavant M, Cox M, Walters D, Boul P, Lu W, Rimberg A, Smith K, Colbert D and Smalley R, *Chem. Phys. Lett.* 303, 125-129, 1999.

28. Venema L, Meunier V, Lambin P and Dekker C, *Phys. Rev. B* 61, 2991, 2000.

29. Ausman K, Piner R, Lourie O, Ruoff R and Korobov M., *J. Phys. Chem. B* 104, 8911, 2000.

CHAPTER 2

DIELECTROPHORESIS AND PHAGE DISPLAY

Dielectrophoresis and phage display are introduced in this chapter since we implement these methods in the following chapters. Dielectrophoresis is used to manipulate nanoparticles and biomolecules such as DNA and proteins while phage display is to investigate the interactions between carbon nanotubes and peptides without the assistant of an electric field.

2.1 Dielectrophoresis (DEP)

As we all know, there is no force excerted on a neutral particle in the uniform electric field although the particle experiences the polarization as shown in figure 2.1. However, it is different in the case that the field is non-uniform: there is net force on the particle. This phenomenon is called dielectrophoresis which is first coined by Pohn in 1951[1]. Such a phenomenon was observed way back to at least 600 BC when people noticed that the amber rubbed with fur could attract light materials[2]. This is Dielectrophoresis in the air or vaccum (since the dielectric constant of air is very close to that of vaccum).

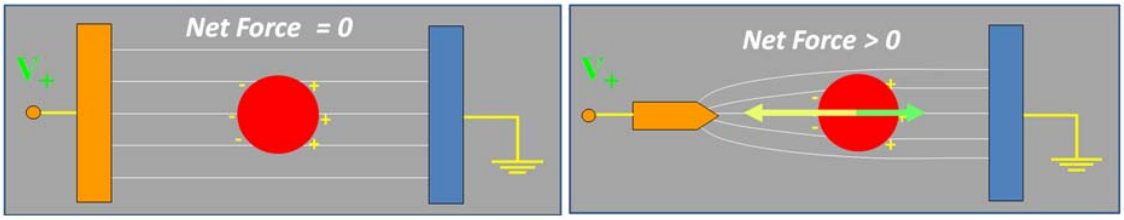

Figure 2.1 Particles in the uniform and nun-uniform fields

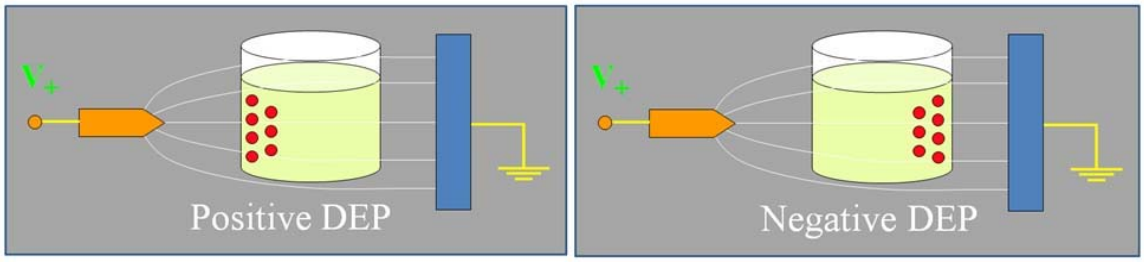

Figure 2.2 Positive and negative DEP

It is a little complicated in the solution. The particles experience the forces with different directions depending on their polarizability. The phenomenon is called positive DEP if the particles move toward the stronger electrical field, negative DEP if toward the weaker electrical field. See figure 2.2.

In a nun-uniform electric field, the force on an induced dipole due to the charge separation of a particle is known as

$$\vec{\mathbf{F}} = (\vec{\mathbf{p}} \cdot \boldsymbol{\nabla})\vec{\mathbf{E}}$$

where $\vec{\mathbf{p}}$ is the induced dipole moment and $\vec{\mathbf{E}}$ is the electric field.

For a spherical particle, the force can be expressed further as following,

$$\vec{\mathbf{F}} = 2\pi\alpha v\varepsilon_m \vec{\nabla}\left(\vec{\mathbf{E}} \cdot \vec{\mathbf{E}}\right)$$

where $\boldsymbol{\varepsilon_m}$ is the dielectric constant of medium, $\mathbf{v}$ is the volume of the particle and $\boldsymbol{\alpha}$ is known as the Clausius-Masotti factor:

$$\boldsymbol{\alpha} = \mathbf{Re}\left(\frac{\varepsilon_p^* - \varepsilon_m^*}{\varepsilon_p^* + 2\varepsilon_m^*}\right)$$

in which $\boldsymbol{\varepsilon_p^*}$ is the dielectric constant of the particle and the star (*) denote the complex quantity of the dielectric constants.

For this technique to be effective in the applications, the DEP force must overcome the Brownian motion which is inverse proportional to the size of the object to be manipulated. Since the gradient of the electric field is very large near the tip of small electrodes, it is

promising to use micro or even nano-fabricated electrodes to manipulate the objects with the technique of dielectrophoresis. In chapter 3 and 4, we demonstrate that nanoparticles and biomolecules are manipulated using dielectrophoresis.

2.2 Phage display

Phage display is a key method for finding ligands for proteins including antibodies and enzymes from the biologists' point of view. It has also been widely used to find ligands for non-protein or inorganic materials recently. Its principle is based on the connection between genotype and phenotype that enables large libraries of proteins to be screened via in vitro selection (or panning) followed by DNA sequencing of binding phage[3,4].

Filamentous phages are ideal and commonly used as cloning vehicles in the display technique. They have small genome that tolerates insertions into non-essential regions. Among many filamentous phages, bacteria-phage M13 is generally used for building a diverse random library. M13 is a virus about 930 nm long and 6.5 nm in diameter. It is made up of a 6400-nucleotide single-strand DNA (ssDNA) encapsidated with coated proteins. The coated proteins are composed of 2700 copies of α-helix major coat protein pVIII, 5 copies each of pVII and pIX on one end and 5 copies each of pIII and pVI on another end.

The most commonly used coat protein for display is pIII, which is responsible for binding to the f-pilus of the *E. coli* bacterial for phage infection. The binding causes the f-pilus to retract into the *E. coli*. The phage then penetrates into the cytoplasmic membrane. The infection process is not fully understood yet, but it must involve a translocation process

of the viral ssDNA into the bacterial cytoplasm where the bacterial proteins (host RNA and DNA polymerases and topoisomerase) replicated the DNA and phage proteins.

After it enters into the host, the ssDNA is coverted to a double-stranded form, which is used as the template for the production of all the phage proteins. Meanwhile, the double-stranded form is also duplicated and used as the template for the production of a large amount of new ssDNA. In this way, all the components of new phage particles are accumulated inside the host bacterium. The newly formed proteins and ssDNA are then packaged and extruded through the bacterial membrane.

The Phage Display PhD-12 Library from New England Biolabs is a commercially available library and has been used in our experiments. The library contains 10^9 12-mer random peptides linearly displayed on the pIII coated protein. The phage has been genetically inserted a lacZ gene into the genome. The lacZ gene encodes for the β-galactosidase, an enzyme that cleaves X-gal (4-chloro-3-indolyl-β-D-galactoside) when IPTG (Isopropyl-β-D-thiogalactopyranoside) is present and produce insoluble blue 5,5'-dibromo-4,4'-dichloro-indigo. See Figure 2.3.

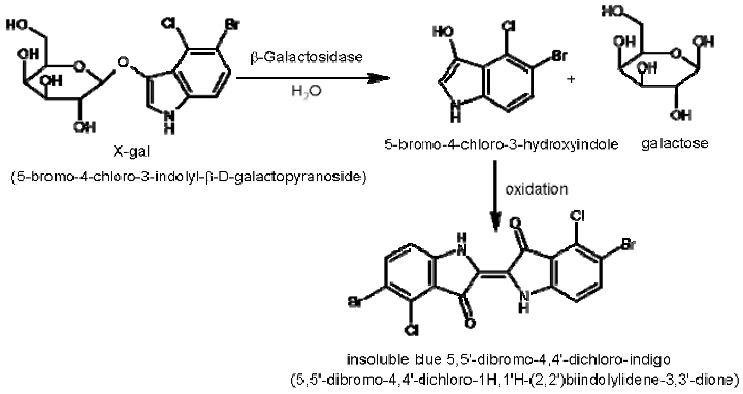

Figure 2.3 Reaction of IPTG. Image from http://en.wikipedia.org/wiki/X-gal.

This reaction is very useful in the titering process which allows us to quantify the number of the phages that are eluted or amplified during the experiments. It is worth to mention

that the bacteria without infection will not produce blue plaques since the ER27 host strain has no lacZ gene. This ensures that all the blue plaques are due to the infection of phages.

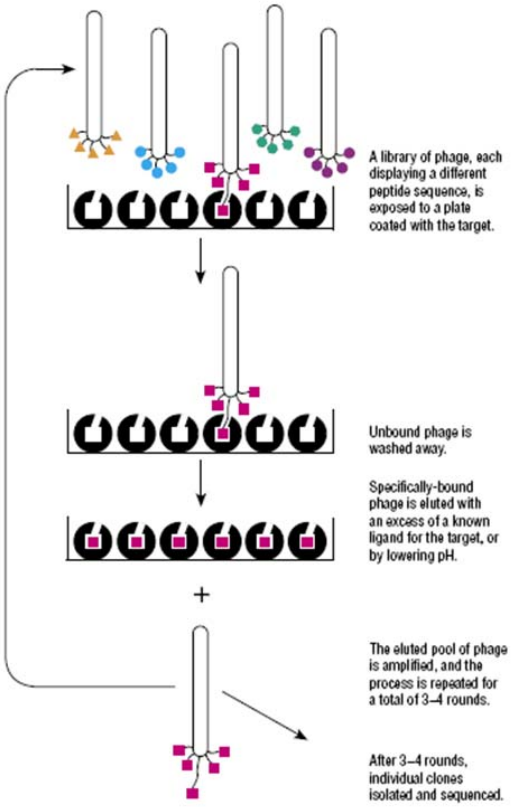

Figure 2.4 Panning with Ph.D peptide display. Image from reference 3.

In the phage display experiments on the traditional target and many inorganic materials, a 10 µl of NEB library is first diluted with 1 ml detergent solution, 0.1% TBST (Tris-buffered saline with 0.1% tween-20) and then the pre-blocked target are incubated in the phage solution for one hour. The process is also called *in vitro* panning. See Figure 2.4. The non-binding phages are dumped away and the target sample is washed with 0.1% TBST five times. The detergent solution is used to remove the non-specific binding (NSB)

phage. An elution buffer, usually glycine-HCl with pH 2.0-3.0, is used to release the bound phage, followed by neutralization of the eluted phage with Tris-HCl (pH 9.1). The eluted phages are titered and then amplified by putting it in the *E. coli* culture (early-log). A 1 μl amplified phage should be titered to make sure that a same amount of phages are used for the next round. The processes of panning, washing, elution and amplification are repeated at least three times to achieve the binding motif. The input vs. output ratio can be calculated by the number of the eluted phages devided by the number of the input phages. 10 blue plaques in the plate for the last round titering are randomly picked and Their DNA are purified and amplified with PCR. The DNA sequences are analyzed to see if there is a binding motif achieved. If not, the extra rounds of phage display experiments should be performed until a motif is achieved.

References

1. H. A. Pohl, *J. Appl. Phys*., 22, 869, 1951.
2. P.J. Burke, "Nano-dielectrophoresis: Electronic Nanotweezers, "*Encyclopedia of Nanoscience and Nanotechnology*, Editor H.S. Nalwa, v. 6, p. 623-641(2004).
3. New England BioLabs Inc manual, “Ph.D-12 Phage Display Peptide Library Kit”.
4. G.P Smith and V.A. Petrenko, Chem. Rev. 97, 391-410, 1997.

CHAPTER 3

ELECTRONIC MANIPULATION OF DNA, PROTEINS, AND NANOPARTICLES FOR POTENTIAL CIRCUIT ASSEMBLY

3.1 Introduction

Using gold electrodes lithographically fabricated onto microscope cover slips, DNA and proteins are interrogated both optically (through fluorescence) and electronically (through conductance measurements). Dielectrophoresis is used to position the DNA and proteins at well-defined positions on a chip. Quadrupole electrode geometries are investigated with gaps ranging from 3 to 100 μm; field strengths are typically 10^6 V/m. 20 nm latex beads are also manipulated. The electrical resistance of the electronically manipulated DNA and proteins is measured to be larger than 40 MΩ under the experimental conditions used. The technique of simultaneously measuring resistance while using dielectrophoresis to trap nanoscale objects should find broad applicability.

3.1.1 Motivation

The development of lithographic fabrication techniques has lead to astounding advances in integrated circuits, but at the same time the limits of lithography prevent nanometer scale electronic devices from being economically manufactured. This has led to proposals

for alternative nano-manufacturing technologies based on "bottom-up" chemical self-assembly techniques.

Two key challenges in the manufacturing of sub-lithographic size electronic devices (i.e., molecular electronics[1]) are 1) Chemical (i.e. bottom-up) control of the electronic properties of the circuit elements, and 2) Electrical connection to the macroscopic world. One approach to the challenge of chemical control is *de-novo* design of unique chemistry for electronics applications[2-3]. An alternative approach is to build on 4 billion years of evolution and use or mimic existing biochemistry, using DNA as a template for chemically programmed assembly of molecular scale devices. Recently several groups have made important progress in using DNA as a template for the construction of higher order structures[4-7]. Because of the attractiveness of the second approach we have decided to concentrate on the electronic manipulation and interrogation of DNA and proteins in this work.

The second challenge of making an electrical connection to the macroscopic world to date has mostly been achieved passively. Much work to date on single molecule devices involves passive diffusion of molecules to small, albeit lithographically fabricated electrodes followed by passive covalent bonding to the electrode[8]. It would be a distinct advantage if this assembly process could be actively, electronically controlled.

3.1.2 Dielectrophoresis

Dielectrophoresis (hereafter DEP) is an electronic analog of optical tweezers using audio frequency, RF, and microwave electric fields generated from microfabricated electrodes on a chip. An ac electric field induces a dipole moment which, in the presence of a field

gradient, experiences a force towards either the high-field intensity region (positive DEP) or the low-field intensity region (negative DEP). Several recent reviews more thoroughly describe the many applications of DEP at the micron, sub-micron, and nanometer scale[9-15]. As with optical tweezers, for DEP to be of use it must dominate the thermal Brownian motion. It can be shown that the force acting on a spherical particle (the DEP force) is given by[16-17]

$$\vec{F}_{DEP} = 2\pi v \varepsilon_m K(\omega) \vec{\nabla}\left(\vec{E}^2_{RMS}\right), \tag{1}$$

where v is the volume of the particle, E_{RMS} the RMS value of the electric field (assuming a sinusoidal time dependence), and K(ω) is a (frequency dependent) factor which varies between -0.5 and +1.0, depending on the difference between the medium and particle dielectric constant. It is defined as:

$$K(\omega) \equiv \mathrm{Re}\left[\frac{\varepsilon_p^* - \varepsilon_m^*}{\varepsilon_p^* + 2\varepsilon_m^*}\right], \tag{2}$$

where ε^* is the (complex) dielectric constant of the particle or medium. It can be related to the conductivity σ and angular frequency ω through the standard formula

$$\varepsilon^* \equiv \varepsilon - i\frac{\sigma}{\omega}. \tag{3}$$

K(ω) is known as the Clausius-Mossitti factor. If K(ω) is positive, then the particle is attracted to regions of high electric field intensity. (This is called positive DEP.) If K(ω) is negative, then the particle is repelled from regions of high electric field intensity. (This is called negative DEP.) Since K(ω) is frequency dependent, both positive and negative DEP can be observed in the same system by varying the frequency.

Although the above analysis assumes a harmonic field, the physical effect is present for dc electric fields as well: a dc electric field can induce a dipole moment, which then experiences a force in the presence of a field gradient. We term this effect *dc DEP*.

In principle, quantitative measurements of the force predicted by Eq. 1 are possible. However, a more direct measurement often used is the frequency at which the force changes from positive to negative DEP. In experiments, the frequency is varied until the particle motion is no longer towards low-field intensity, and instead is towards high-field intensity regions; this is straightforward to observe. For a spherical particle, it can be shown that this frequency, called the "crossover frequency", is given by[18]:

$$f_{x-over} = \frac{1}{2\pi}\sqrt{-\frac{(\sigma_p - \sigma_m)(\sigma_p + 2\sigma_m)}{(\varepsilon_p - \varepsilon_m)(\varepsilon_p + 2\varepsilon_m)}} \qquad (4)$$

In eqs. 1-3, the values of ε^* and σ are assumed to be the bulk values. For nanoparticles and biological nanostructures such as DNA, a significant fraction of the atoms of the "particle" reside on the surface; in addition, the particles can be charged. For example, at neutral pH, DNA is negatively charged. Protons and any other positively charged counter-ions are attracted and form a counter-ion cloud. Clearly, the corresponding electrical double-layer (consisting of the positively charged counter-ion cloud and the negatively charged particle) can have a significant effect on DEP.

The effects of the double layer on the dielectric properties of colloidal solutions of dielectric particles was considered theoretically on very general grounds in several key papers in the 60's and refined in the 80's[19-23]. While these authors concentrated on dielectric properties, they did not discuss DEP. In the late 90's, Green, Morgan, Hughes, and co-workers performed extensive experimental investigations on latex beads down to

93 nm in diameter, varying the frequency, surface chemistry, and electrolyte conductivity[24-32]. They based the interpretation of the experiments on the earlier theories of the charge double layer. The conclusions of their results can be summarized as follows: The effects of the charge double layer are to incorporate a surface conductance due to the motion of either bound counter-ions (the Stern layer) or diffuse counter-ions, with numerical value given by K_s. Eqs. 1-4 are still valid, provided that the total particle conductivity in Eq. 3 be replaced with

$$\sigma_p = \sigma_b - \frac{2\kappa_s}{a}. \qquad (5)$$

Here a is the particle radius, and σ_b the bulk conductance. Generally speaking, Eq. 5 should only be used if the frequency is less than the inverse of the diffusion time of ions across a distance of order a. If this is not the case, then Eq. 5 should be modified.

For this force to be effective it must overcome the Brownian motion, which can be treated as a random force whose maximum value is given roughly by

$$F_{thermal} = k_B T / \sqrt[3]{v}, \qquad (6)$$

where k_B is the Boltzmann constant, T the temperature, and v the particle volume. This sets a rather strict requirement on the minimum particle size that can be manipulated, and very large electric field gradients are needed to manipulate nano-sized particles. Microfabricated electrodes can be used to generate the required field gradients, although the lower limit on the particle size that can be manipulated is still under experimental investigation[33].

3.1.3 Dielectrophoretic impedance spectroscopy

While deterministic motion of individual molecules due to DEP is difficult to achieve due to Brownian motion, it is still true that the non-uniform ac and dc electric fields establish *some* force, which, even though less than the thermal Brownian motion, will still cause a tendency for molecules to move in a certain direction, depending on the geometry of the electrodes. The quantitative study of these effects has been termed ``molecular DEP'' [16]. The establishment of impedance spectroscopy essentially consists of measuring the ac impedance between two electrodes at a probe frequency while DEP is used to manipulate objects at a separate frequency. This technique was originally pioneered over 50 years ago.

The geometry originally studied consists of two concentric cylinders with the molecules dissolved in a solution in between the cylinders. If the density of the molecules as a function of the radial distance changes, this changes the dielectric constant as a function of the radius, and hence the capacitance from the inner to the outer cylindrical electrode. This can be termed a form of dielectrophoretic impedance spectroscopy.

In 1954, Debye and co-workers used dc DEP of polystyrene (molecular weight 600,000) in cyclohexane[34-35]. They used a dc non-uniform electric field in a cylindrical geometry and monitored the capacitance change by measuring the shift in the resonant frequency of an LC circuit; similar studies were carried out by Prock in 1960[36].

In 1955, Losche used ac DEP to study nitrobenzene in carbon tetrachloride, and poly(vinyl acetate) in nitrobenzene[37]; however both have permanent (instead of induced) dipoles. In 1973 Eisenstadt studied DEP and measured the diffusion constant of the biopolymers poly-γ-benzyl-L-glutamate (PBLG, M.W. 120,000) and poly-n-butyl

isocyanate dissolved in ethylene dichloride (Edc)[38-39]; both have permanent dipoles. By measuring the time-dependence of the concentration change of the PBLG concentration due to the dielectrophoretic force, Eisenstadt was able to determine its diffusion constant. Recently, Milner and co-workers have extended dielectrophoretic impedance spectroscopy to larger particles which can be deterministically manipulated with DEP. They used DEP to position bacteria[40-41] or 20 nm latex beads[42] with high frequency (kHz-MHz) electric fields, and simultaneously measured the low frequency (~100 Hz) impedance between two electrodes.

Thus, there is an extensive history and established technology to use DEP to manipulate a variety of objects (molecules, nanoparticles, cells) at one frequency, and to use a different probe frequency to measure the impedance change when the objects are moved. However, all of the examples cited above cause a change in the *capacitance* between the electrodes. Hence, the probe frequency could not be too low. Our work in this manuscript addresses a related but somewhat different goal: We are interested in using DEP to fabricate *circuits* that function at dc. As we discuss next, there are a many examples from the literature demonstrating that this can be done.

3.1.4 DEP for nano-circuit fabrication

To date there have been several examples of the application of DEP to circuit fabrication at the nanometer scale. Suehiro measured the resistance and capacitance between two electrodes at 100 kHz before and after bacteria cells were trapped using DEP[43]; he modeled each cell as a resistor in parallel with a capacitor and found good agreement with experiment: the cells formed "pearl chains" and bridged the gap between the two electrodes. Bezryadin used (dc) DEP to trap a 20 nm Pd nanoparticle between a two

electrodes, allowing current to flow at dc[44-45]. Bezryadin later used DEP to trap carbon nanoparticles between electrodes in pearl-chain formation, and measured non-linear dc I-V curves due to Coulomb blockade[46]. Amlani used DEP to trap a Au nanoparticle coated with a self-assembled monolayer (SAM), and he observed negative differential resistance at dc from electrode to electrode due to the SAM[47]. Porath used dc DEP to trap short strands of DNA and measured the conductance of DNA so trapped[48]. Velev used DEP to assemble microwires from nanoparticles and measured dc current through these[49-50]. We recently use carbon nanotubes as electrodes to assemble gold nanowires from nanoparticles[51]. Several groups have used both ac and dc DEP to trap single walled and multiwalled carbon nanotubes between electrodes which then carry dc current[52-59]. Smith used DEP to assemble gold nanowires across electrodes, which then carried dc current[60]. Duan assembled functional crossbar networks of semiconducting nanowires using dc DEP[61]. Lee and Bashir measured Si resistors at dc after using ac DEP to position them between electrodes[62]. To date no authors have used ac DEP to manipulate DNA then measure conductance between two electrodes, and no authors have measured any protein conductance after DEP manipulation, as we do in this manuscript. Our work in this manuscript thus represents the first step towards extending DEP for circuit fabrication into the molecular domain.

3.1.5 DNA Manipulation: Washizu

Starting in 1990, Washizu and Kurosawa began studies on manipulating and stretching DNA in high intensity ac electric fields between 40 kHz and 2 MHz generated by microfabricated electrodes[63]. They found that a high-frequency electric field would stretch DNA into a line, whereas its natural configuration is coiled. In 1995, Washizu and

co-workers described several possible applications of this technology[64], such as size-sorting long DNA (length > 10 kbp) which is difficult for conventional gel electrophoresis, laser cutting of DNA with spatial resolution determined optically, and measurements of the rate of exonuclease DNA digestion. Further work by Washizu and co-workers used DEP and showed, for example, that RNA polymerase actually slides along DNA molecules during genetic expression[65-67], that DEP works at the single DNA molecule level, not on aggregates[68], restriction enzyme cutting of DNA oriented using DEP[69], and the polarization of the fluorescent emission from dielectrophoretically stretched DNA[70]. In spite of all this outstanding experimental work, very little explanation was given of the electrical double layer in the DNA.

3.1.6 DNA Manipulation: Other groups

Since Washizu's pioneering experiments in the early 1990's, several other groups have convincingly demonstrated the dielectrophoretic manipulation of DNA. Asbury and co-workers were able to manipulate DNA with a floating Au electrode geometry[71-72] using frequencies between 5 Hz and 2 kHz. In contrast to Washizu's experiments which clearly showed DNA to be stretched by DEP using higher frequencies, Asbury found for the lower frequency DEP can position DNA but does not stretch it.

Ueda and co-workers found that DNA could be stretched but not positioned when a polymer solution (polyacrylamide) was used[73-74]; 10 Hz was the frequency used. They also found the required electric field strength to be 100 times smaller than that of Washizu and Asbury.

In another recent work with floating electrodes, Chou and coworkers[75] used *insulating* posts fabricated with micromachining techniques, and electrodes external to the device.

The slightly conductive solution served to enhance the electric field near the gaps between the posts, and DNA was found to be trapped there for voltages on the electrodes of roughly 1000 V and frequencies between 50 Hz and 1 kHz. The corresponding electric field strength was 10^5 V/m. In this work, the DNA was apparently not stretched at all, presumably because of the constricted geometry used. In contrast to the work of Asbury, Chou found that the trapping force increased with increasing frequency, and also calculated that the trapping force was roughly one femtonewton.

In recent work[76] Tsukahara and co-workers studied DEP of single DNA molecules using frequencies between 1 kHz and 1 MHz and field strengths around 10^4 V/m, using quadrupole electrode geometries. They found that the DNA underwent positive DEP (i.e. it was attracted to the high field regions near the edges of the electrodes) for frequencies between 1 kHz and 500 kHz, and negative DEP between 500 kHz and 1 MHz, in contrast with the findings of previous work. This is to date the only reported observation of negative DEP of DNA. Additionally, Tsukahara did not observe any stretching of the DNA with the application of an ac electric field.

Namasivayam and co-workers recently used 1 MHz ac fields and thiol modified DNA to trap single DNA molecules to gold electrodes; they studied the stretching as a function of polyacrylamide concentration[77]. Holzel and co-workers also recently used DEP at 2 MHz and selective electrode functionalization to vectorially orient DNA molecules which bridged a gap between electrodes[78-79]. Germishuizen and co-workers oriented (stretched) surface immobilized DNA using 80 kHz – 1.1 MHz DEP[80-81]. Recently, Dewarrat and coworkers optimized the geometry of the lithographic structures to favor a precise positioning of DNA using 100 kHz – 1 MHz[82].

The detailed mechanisms for the frequency dependence, electric field dependence, concentration dependence, pH and ionic dependence of the dielectrophoretic manipulation of DNA are still not explained in a systematic, quantitative way, and many of these dependences have yet to be quantitatively measured. In addition, none of these authors have measured the electrical properties of the DNA after manipulation.

3.1.7 DNA and proteins: electrical properties

Thus, while most of this research work focused on manipulating DNA and proteins, investigation of their electrical properties is still in its infancy. In 2000, Porath and co-workers used positive dc DEP to putatively trap 10 nm long poly(G)-poly(C) double strands of DNA between Pt electrodes with 8 nm spacing[48]. Through a series of control experiments, Porath concluded that the trapped object was indeed DNA, and that its electrical properties were semiconducting. Many other researchers up to and since then have considered the electronic properties of DNA as a molecular wire. Since then, experiments performed by different research groups have indicated that DNA has insulating, semiconducting, metallic and even superconducting properties[48,83-88].

These differing results of the electrical properties of DNA indicate that effective methods should be set up for the measurements. As for the electrical properties of proteins, these biological nanostructures have yet (until now) to be interrogated electrically. Our work in this chapter represents the first step in this direction. Since various proteins have many differing chemical and mechanical properties, it can be argued that their electrical properties will be even more diverse (and hence interesting) than those of DNA.

3.1.8 This research work

In this work, a technique is presented that may be useful for the electronic control of manufacturing devices at the molecular scale by controlling the position of DNA and proteins on a chip to fabricate simple electrical circuits (a conductor bridging a gap). We apply our technique to DNA and proteins to measure, for the first time, the conductance of DNA and proteins trapped between two electrodes using DEP by *in situ* monitoring the impedance change of the DNA and protein solutions in both solution and dry states. This technique contains the rudimentaries of single molecule transistor fabrication with an essentially nano-electrochemistry approach[89-90]. What is new about this work is:

1) It is the first measurement of the conductivity of DNA after ac DEP manipulation
2) It is the highest frequency DEP experiment to date on DNA by an order of magnitude
3) It is the first ever measurement of the electrical properties of any protein
4) It is the first measurement of the crossover frequency from positive to negative DEP of 20 nm diameter nanoparticles (previously the crossover frequency was measured for 93 nm nanoparticles and aggregates of 14 nm beads)
5) It is a new application of an old technique (DEP) to fabricate nano-circuits using ac voltages at the molecular scale.

In Figure 3.1, we show a scale drawing of the three objects manipulated in this article: nanoparticles, DNA, and BSA protein. Although we are taking the first initial steps in this work, it should be noted that these are mere "baby steps" towards electronic control of the assembly of matter into circuits at the molecular scale.

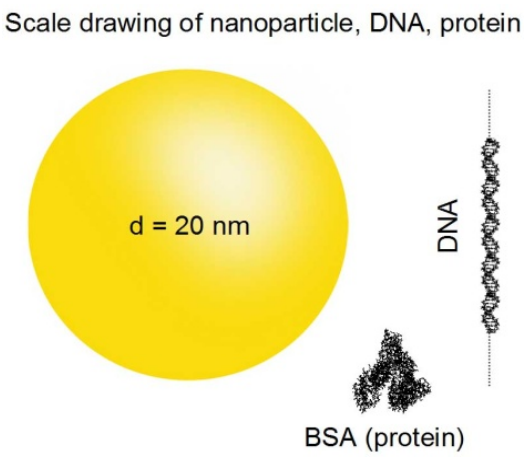

Figure 3.1: Scale drawing of objects manipulated in this chapter.

3.2 Materials and methods

3.2.1 Electrode design and fabrication

For our experiments, electrodes were fabricated using photolithography onto microscope cover slides. Ti(10 nm)/Au(100 nm) bilayers were deposited with electron-beam evaporation and lifted off in acetone. The geometry of the electrodes was designed for both positive and negative DEP experiments. For negative DEP, Huang and Pethig have shown that a planar, "quadrupole" electrode geometry allows the trapping of particles under the influence of negative DEP in the center of the electrodes, called the "trap." [91] This is because there is an electric field gradient minimum in region of the center of the electrodes, and particles undergoing negative DEP are repelled from the higher field regions.

We have also performed numerical simulations for our electrode geometry, which is slightly different from the geometry considered by Huang. We find that the electric field gradient is maximum in the region closest to the electrode edges. Thus, for particles which undergo positive DEP, they should be attracted to those regions.

3.2.2 Sample preparation

Solutions containing either fluorescently labeled λ-phage DNA, BSA protein, or 20 nm latex beads were prepared as described below. An aliquot was placed on the cover slip with electrodes, which is then covered by a second slip. This configuration was necessary for the inverted microscope configuration used. An RF function generator (Stanford Research Systems model DS 345) was used to apply electric fields in the frequency range of 10 kHz to 30 MHz, and applied voltages of up to 10 V_{pp}.

3.2.3 Optical interrogation

The solution was imaged through an inverted Nikon TE200 microscope, equipped with a 40x/1.3NA objective. Fluorescent images used epi-illumination with a mercury arc lamp providing the excitation. A back-illuminated, slow-scan, cooled CCD camera (AP7P, from Apogee Instruments) captured the images.

3.2.4 Electronic interrogation

After trapping, the low frequency (13 Hz) conductance between two electrodes was measured simultaneously while applying the ac electric field. The circuit used for the measurement is shown in Figure 3.2. The high frequency electric field was used to trap the DNA or protein between the electrode gaps. A small amplitude, ac voltage was simultaneously applied and a lock-in-analyzer (Stanford Research Systems model SR830) simultaneously measured the 13 Hz ac current. The 13 Hz current was monitored continuously as the solution dried in order to measure the conductance in both the wet and dry state.

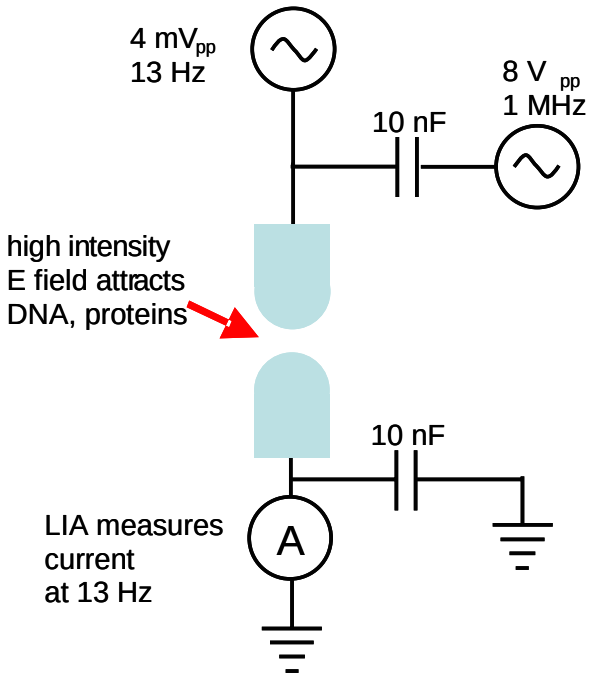

Figure 3.2: Circuit for conductance measurements.

In the experiments described in this chapter, the measured conductance corresponds to a large number of molecules trapped electronically between the electrode gaps. While the fluorescence imaging experiments clearly and unambiguously demonstrate the presence of a large number of molecules of either DNA or proteins present in the gap between the electrodes, it remains for future work to provide more quantitative estimates for the number of molecules trapped and to push to the single molecule limit[33]. In Figure 3.3, we show a schematic physical picture of the process of the DEP trapping.

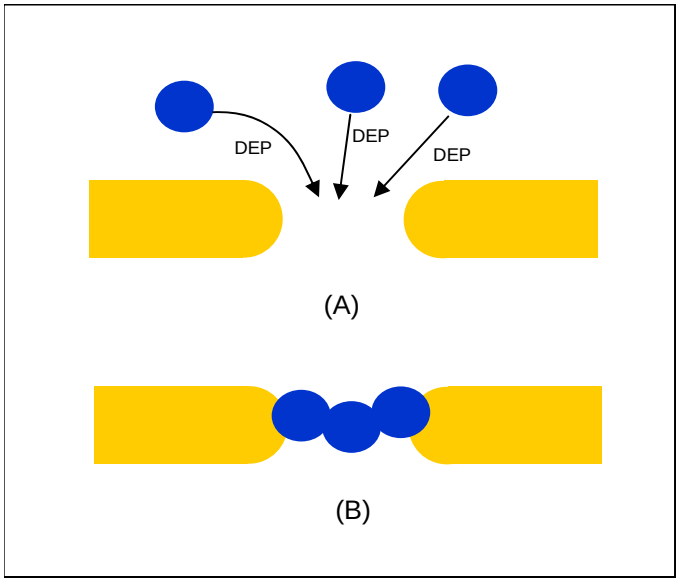

Figure 3.3: Schematic of DEP trapping process. In this figure, the blue balls represent proteins and DNA.

The impedance between the electrodes consists of two parts, which we indicate in Figure 3.4: First, there is the impedance of the electrolyte, which is a complicated function of frequency. In particular, at low frequencies, this impedance is dominated by the capacitance of the electrode-electrolyte interface. This impedance, which has been described in detail in[90], is not of prime interest in our work here. We are primarily interested in the fabrication of circuits, which can function even in the dry state, and at dc. The electrode-electrolyte impedance at dc forms a cell (battery) which we are not concerned with in this work.

If the objects manipulated by DEP come into physical contact with both electrodes, then there will be a second, parallel conduction path, due to the impedance of the object *itself*. Generally, this impedance will dominantly be *resistive*, and hence relatively frequency independent. Because we are interested primarily in this resistive impedance, we chose a low probe frequency. However, we choose not to probe at dc, because the

electrochemical effects (polarization of the electrode) at dc would mask the resistive impedance we are interested in. Thus, the frequency of 13 Hz was chosen to measure this second, resistive component.

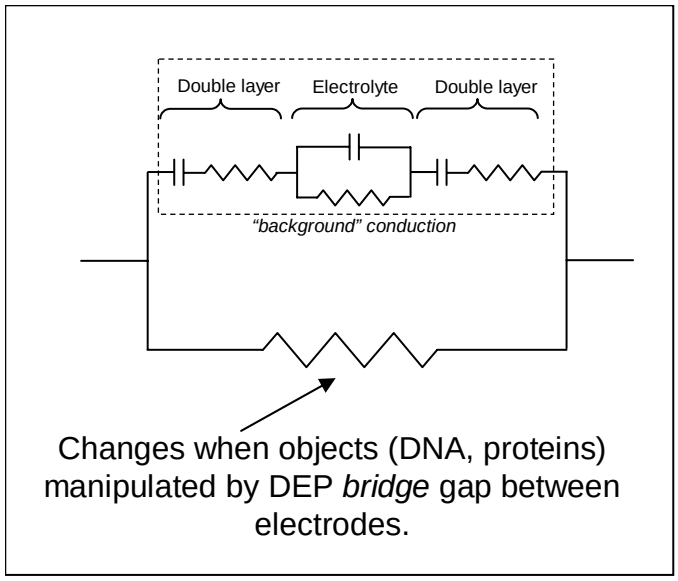

Figure 3.4: Effective circuit model for objects trapped using DEP between electrodes.

3.3 Results: DNA

3.3.1 DNA: optical measurements

The DNA used in the experiments was λ-phage DNA (48.5 kilo-base pairs). The DNA solution was prepared as follows: λ-phage DNA (Promega Corporation, Madison, WI) was purchased in a buffer solution of 10 mM Tris-HCL, 10 mM NaCl, 1 mM EDTA, at a concentration of 500 μg/ml. The solution was diluted 5 x 10^5 times with D.I. water. SYBR green was then added to the solution for the fluorescence measurements. The suspension conductivity was 1 mS/m.

We observed that DNA under our experimental conditions undergoes positive DEP (i.e. is attracted to high electric field intensity regions) for a range of frequencies between 100 kHz and 30 MHz. Below 100 kHz, no effect was observed. We did not observe DNA to undergo negative DEP under our experimental conditions. We show in Figure 3.5 images of successive on/off/on/off conditions of DNA which has been trapped in the high-field region between electrodes with a 10 μm gap. We clearly observe positive DEP (i.e. the DNA is attracted to high electric field intensity regions) over a range of frequencies between 100 kHz and 1 MHz.

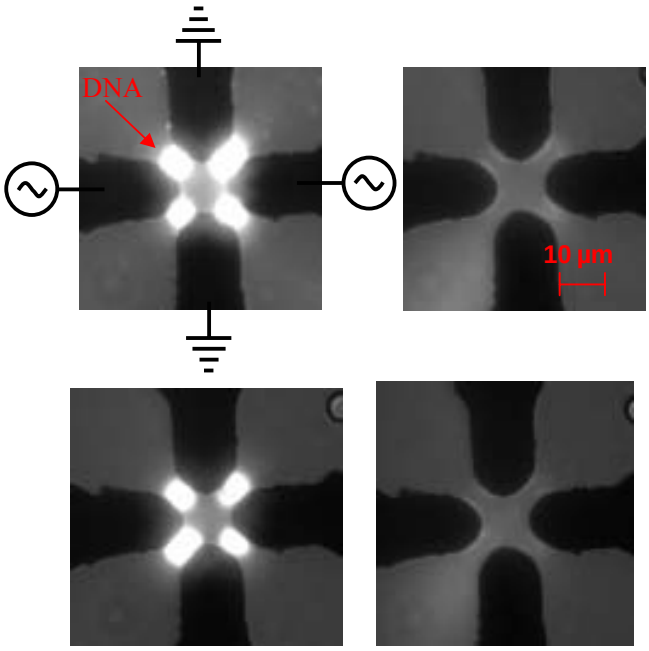

Figure 3.5: Images of fluorescently labeled DNA. The four images were taken in on/off/on/off sequence in a time span of about 30 seconds. The applied voltage was 1 MHz, 8 V_{pp}.

We have repeated this experiment dozens of times with electrodes with central gaps of 5 μm, 10 μm and 20 μm. With four electrode geometries with 50 μm gaps, we were unable to see any effect of the electric fields on the DNA for applied voltages of up to 8 V. This

is consistent with the scaling arguments presented above: large electrodes are less effective in trapping nano-sized objects than smaller electrodes. We have also been able to trap DNA using interdigitated, castellated electrodes with 10 μm gaps. DNA was only observed to undergo positive DEP with those electrodes, as well.

3.3.2 DNA: electronic measurements

λ-phage DNA stretched is 17 μm long, but in its native state it is a randomly coiled ball about 2-4 μm in diameter. In our experiments the gap between the electrodes was less than 5 μm at the nearest point, so we expect that the DNA is stretched out and connects to both electrodes.

In a separate experiment, we applied an aliquot of solution to the electrodes and monitored the 13 Hz current as per the circuit diagram in Figure 3.2. A "background" current of 227 nA was measured in the absence of the high frequency signal, due to the background conductivity of the electrolyte, indicated in the dotted lines in Figure 3.4. This background signal is expected to be only weekly dependent on whether the DNA molecules bridge the gap between the electrodes on the surface of the sample. In fact, the reason we use D.I. water in the experiments presented in this work is to *minimize* this background conductance.

Then, while monitoring the 13 Hz current *in situ*, a 1 MHz ac electric field was applied to trap DNA between the electrodes. Based on the optical interrogation measurements presented in the previous section, we are confident that the DNA is indeed collected between the electrodes. After trapping the DNA with the 1 MHz field, no change in the 13 Hz current was measured within a resolution of 0.1 nA. We monitored the current as the solution dried over a period of 72 hours. After the solution dried the measured current

was below the noise level of the measurement (0.1 nA). This corresponds to an upper limit of 25 nS for the conductance indicated by the large resistor in Figure 3.4 for the DNA. This work represents the first such measurement of the conductance of DNA after trapping with an ac electric field.

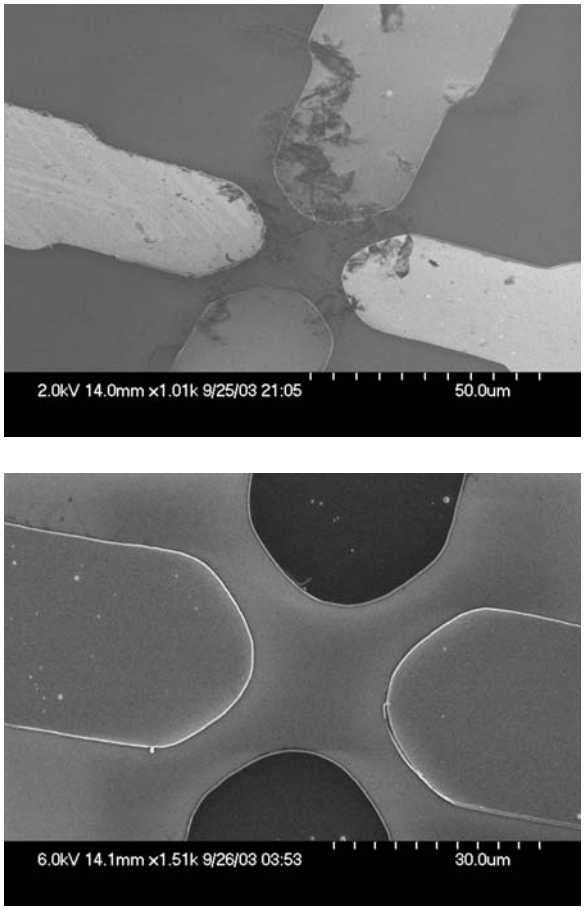

A B

Figure 3.6: A. Sample SEM image after drying when DNA solution was used. B. Sample SEM image after drying when only D.I. water was used.

In order to verify that the DNA is indeed trapped electronically, we have conducted a set of control experiments. An aliquot of DNA solution with a concentration of 10^{-6} μg/ml was dropped onto one sample with quadrupole electrodes. For a control sample, D.I. water was dropped onto a similar set of electrodes. An ac bias of 8 V at 1 MHz was applied to both samples. Both the DNA solution and D.I. water were dried in air while the voltage was still being applied. The samples were then imaged in an SEM; the SEM pictures are shown in Figure 3.6. The dark material between the electrodes shown in Figure 3.6A is not seen in the control electrodes shown in Figure 3.6B. Since the DNA solution is composed of only λ-phage DNA and D.I. water, we believe that the dark material is DNA itself.

3.4 Results: Proteins

3.4.1 Proteins: optical measurements

For the protein experiments, the sample was prepared as follows: Bovine serum albumin (BSA, molecular weight 68kD) labeled with tetramethylrhodamine (Molecular Probes, Eugene, OR) was dissolved in D.I. water at a concentration of 1 mg/ml and centrifuged. The supernatants were diluted to 1 μg/ml with D.I. water. The suspension conductivity was 1 mS/m.

We observed that BSA underwent positive DEP for frequencies between 50 kHz - 5 MHz. Negative DEP was not observed at lower frequencies under our experimental conditions. The frequency range of 200-300 kHz was observed to be most effective at attracting the BSA to the high-electric field regions. We show in Figure 3.7 images of successive on/off/on/off conditions of BSA which has been trapped in the high-field

region between electrodes with a 10 μm gap. We clearly observe positive DEP (i.e. the BSA is attracted to high electric field intensity regions) over a range of frequencies between 50 kHz and 5 MHz. We have repeated this experiment dozens of times with electrodes with central gaps of 5 μm, 10 μm and 20 μm. With four electrode geometries with 50 μm gaps, we were unable to see any effect of the electric fields on the BSA for applied voltages of up to 8 V.

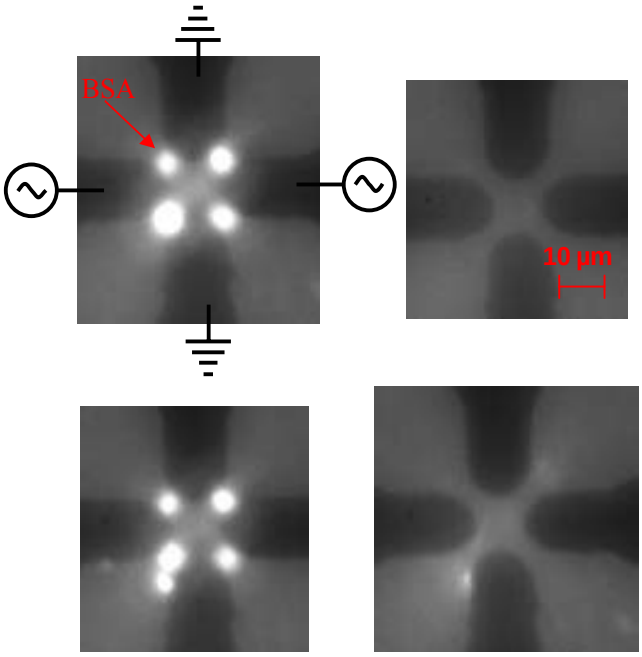

Figure 3.7: Images of BSA protein in a span of about 30 seconds. f=200 kHz, amplitude = 8 V_{pp}.

3.4.2 Proteins: electronic measurements

In its folded state BSA should be roughly spherical in geometry with diameter of order 10 nm. Previous work of Washizu has shown that high intensity electric fields can change the conformational state of certain proteins[93], however the effect of the high-intensity electric field on BSA is unknown. While we were unable to image single BSA molecules

under our current experimental setup, it is clear that a large number of BSA molecules were attracted to the gap between the electrodes. With this in mind we measured the conductance at 13 Hz to determine whether it was possible to electrically interrogate the BSA.

In a separate experiment, we applied an aliquot of protein solution to the electrodes and monitored the 13 Hz current as per the circuit diagram in Figure 3.2. A "background" current of 2.5 nA was measured in the absence of the high frequency signal, due to the background conductivity of the electrolyte, indicated in the dotted lines in Figure 3.4. (This background current was less than the background current in the case of the DNA because we used smaller aliquot of solution). This background signal is expected to be only weakly dependent on whether the protein molecules bridge the gap between the electrodes on the surface of the sample.

Then, while monitoring the 13 Hz current *in situ*, a 1 MHz ac electric field was applied to trap protein between the electrodes. Based on the optical interrogation measurements presented in the previous section, we are confident that the protein is indeed collected between the electrodes. After trapping the protein with the 1 MHz field, no change in the 13 Hz current was measured within a resolution of 1 pA. We monitored the current as the solution dried over a period of 24 hours. After the solution dried the measured current was below the noise level of the measurement (0.1 nA). This corresponds to an upper limit of 0.25 nS for the conductance indicated by the large resistor in Figure 3.4. This work represents the first such measurement of the conductance of any protein after trapping with an ac electric field.

3.5 Results: Nanoparticles

In a final set of experiments we were able to use DEP to manipulate fluorescently labeled latex beads of diameter 20 nm (Molecular Probes, Eugene, OR) suspended in D.I. water. The suspension conductivity was 1 mS/m. Latex beads have served as an ideal test-bed for the use of DEP at the micron and submicron scale[24,25,94] and serve as convincing evidence that under our experimental conditions it is indeed possible to manipulate submicron objects.

For the 20 nm beads, we found that the beads undergo positive DEP for frequencies between 500 kHz and 22 MHz, while above 22 MHz the beads undergo negative DEP. We show in Figure 3.8 an image of beads undergoing negative DEP, with an applied frequency of 22 MHz. The beads are seen to be trapped in the center of the electrodes. In Figure 3.8, we show an image of beads under the influence of positive DEP, where they are clearly seen attracted to the region of high electric field intensity between the electrodes.

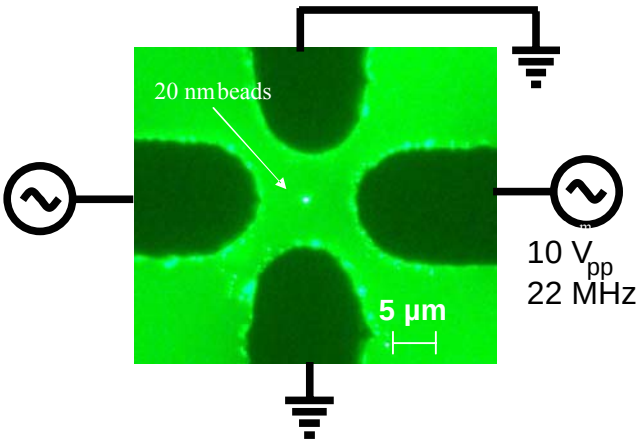

Figure 3.8: 20 nm latex beads shown trapped in the center of the electrodes due to negative DEP.

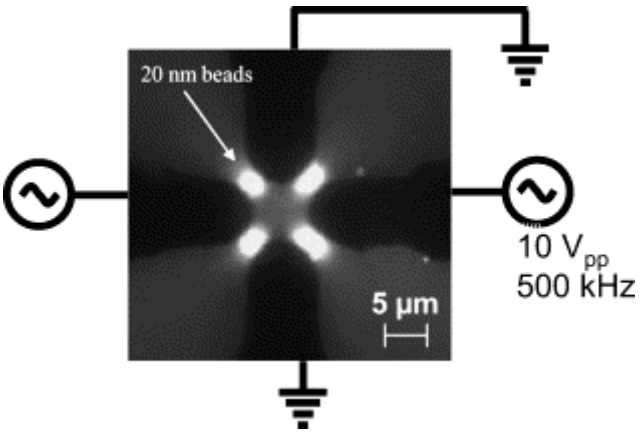

Figure 3.9: 20 nm latex beads shown attracted to high electric field regions between the electrodes.

3.6 Summary of results: DEP Spectrum

In Figure 3.10 below, we show the resulting spectrum for positive vs. negative DEP for the three objects measured. This is the DEP "spectrum".

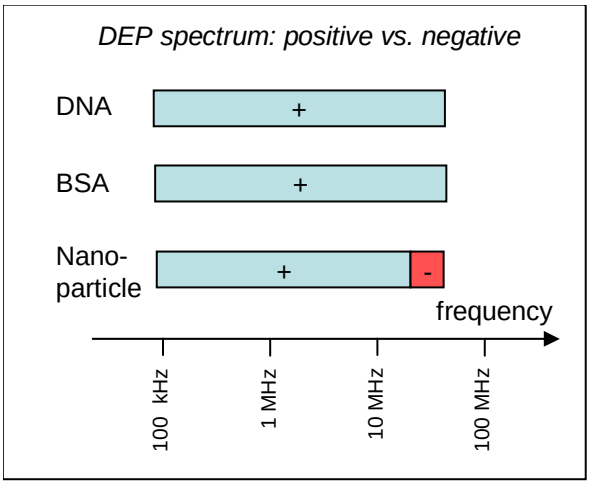

Figure 3.10: DEP spectrum, showing frequency regions where positive (+) and negative (-) DEP were observed. 30 MHz was the upper frequency limit for our electronics.

3.7 Discussion: Nanoparticles

We begin our discussion of the nanoparticle results, as they are the simplest to interpret. A key initial question is whether the nanoparticles form aggregates. Previous research using DEP on 14 nm latex beads found that the particles form aggregates[94], while work on single 93 nm beads was reported in[25]. Because of the spatial resolution limits of optical microscopy it is very difficult to determine if aggregates are formed using optical microscopy alone. However, we have independent evidence that, under our experimental conditions, the 20 nm beads do *not* form aggregates. In a separate experiment[92], we used nanotube electrodes to trap 20 nm beads and then imaged them with a scanning electron microscope. Under the SEM, we see no evidence whatsoever for aggregation. Thus, we believe the 20 nm beads are not aggregated.

The frequency dependence of the nanoparticle experiments is given in Figure 3.10; in sum we find positive DEP at frequencies below 22 MHz and negative DEP at frequencies above 22 MHz. In order to interpret this result, we use Eqs. 1-5 as the basis for our analysis. Our experimental result for the crossover frequency corresponds theoretically to the frequency at which the Clausius-Mosotti factor crosses from positive to negative.

The frequency dependence of the Clausius-Mossotti factor (Eq. 2) is determined by the frequency dependence of the complex medium and particle dielectric constants. The real part of the medium dielectric constant can be taken as 78.5 and independent of frequency over the range of interest. Similarly, the real part of the dielectric constant of the nanoparticles can be taken as 2.55, and independent of frequency over the range of

interest. The frequency dependence of the C.M. factor is thus determined entirely by the imaginary part of the dielectric constants, which we discuss next.

For the medium, the conductivity is known, so the imaginary part of the medium dielectric constant is known. For the nanoparticle, the bulk conductivity is negligible. However, the surface of the nanoparticle has a negative static charge density, which attracts counter-ions from the solution. These can be bound to the surface of the nanoparticle (the Stern layer) or occur as a diffuse cloud. Eq. 5 provides a means of estimating the effect of both these counter-ion concentrations, provided an effective surface conductivity (K_s) is known for these counter-ions. In general predicting the numerical value of K_s is difficult. Green and Morgan measured its value on larger nanoparticles (93 nm – 557 nm) and found it to be of order 1 nS[27]. If we assume this value is appropriate also for the 20 nm nanoparticles in our experiments, we can predict the frequency-dependent C.M. factor for our experiments. This prediction is shown in Fig.11 below. The predicted crossover frequency (which can also be calculated analytically from Eq. 4) of 30 MHz is close to our experimentally measured crossover frequency of 22 MHz. Given the fact that the surface conductivity K_s is not known independently, this is a reasonable agreement with previous experiments and theoretical predictions.

While we do not know whether the surface conductance is due predominantly to the bound or diffuse counter-ions, the agreement between the theoretical and experimental crossover frequency seems to indicate that *bound* counter-ions contribute the dominant portion. The diffuse cloud of counter-ions extends a Debye length between the particle and medium. The Debye length is given by:

$$\lambda_{Debye} = \sqrt{\frac{\varepsilon k_B T}{2e^2 n}} \tag{7}$$

For our solutions, this corresponds to 100 nm, much larger than the particle diameter. In our prediction for the crossover frequency, we have neglected the finite thickness of the diffuse cloud of counter-ions, and we still find reasonable agreement with experiment. The bound counter-ions will not significantly change the effective diameter of the nanoparticle for the DEP crossover frequency used in Eq. 5. This leads us to conclude that bound counter-ions dominate the surface conduction K_s.

Our experiments were performed in a medium with low conductivity, 1 mS/m. Based on Eq. 4, we can predict the dependence of the crossover frequency on the medium conductivity. This prediction, together with our experimentally measured crossover frequency, is shown in Figure 3.12 below. Armed with this understanding of the frequency dependence of DEP of the 20 nm beads and the effect of the charge double layer, we move on next to analyze the experiments on the proteins.

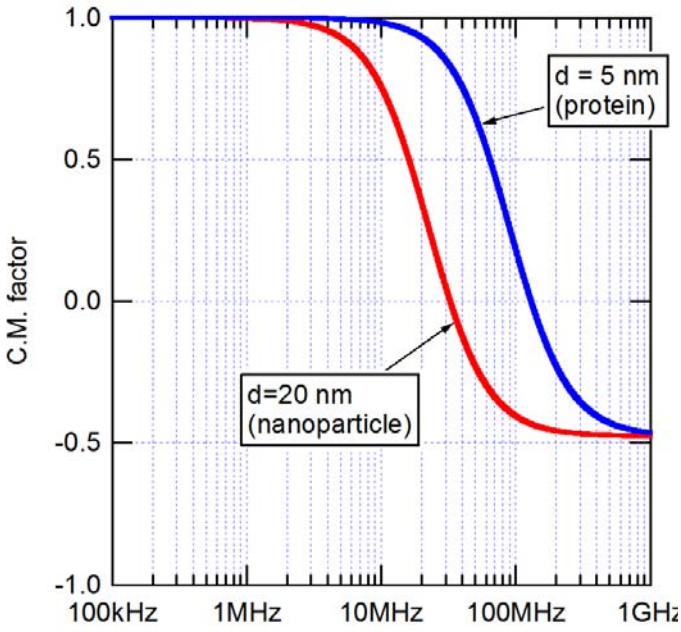

Figure 3.11: Frequency dependence of the Clausius-Mossotti factor, assuming a surface conductance of K_s = 1 nS.

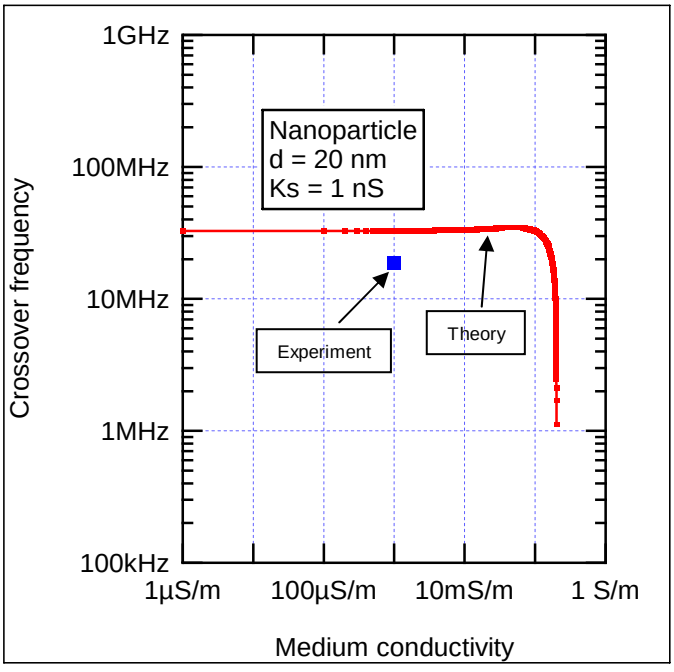

Figure 3.12: Predicted dependence of DEP crossover frequency on suspension conductivity.

3.8 Discussion: Proteins

Our analysis of the protein DEP measurements proceeds along the lines of the 20 nm nanoparticle measurements. For simplicity we model the albumin protein as a sphere of diameter 5 nm; this should be expected to yield semi-quantitative results. Using this model allows us to apply the analysis based on Eqs. 1-6 for spherical particles. For our protein experiments, the charge double-layer and surface conductivity play a critical role. As with the latex bead experiments, the surface conductivity of the bound or diffuse counter-ions is difficult to predict from first principles. If we use our results from the 20 nm latex beads as guide, we can estimate a reasonable value for the surface conductivity of 1 nS. Based on this estimate, and assuming the bulk conductivity of the protein is negligible, we calculate a spectrum for the C.M. factor shown as the blue curve in Figure 3.11. (This curve is insensitive to the numerical value of the real part of the dielectric constant for the protein.) This curve, and also Eq. 4, predicts a crossover frequency of ≈ 100 MHz, which is larger than the frequency range used in these experiments. This is entirely consistent with our experimental results: we observe only positive DEP for the proteins measured up to 30 MHz, i.e. we observe a positive C.M. factor.

We are now in a position to integrate our nanoparticle experiments, those of Green and Morgan, and our protein experiments into a unified understanding of the role of the double-layer and particularly the surface conductance in determining the cross-over frequency for the application of DEP to nanoparticles. In Figure 3.13 we plot our measured crossover frequency (in the low suspension-conductivity limit) as a function of particle diameter, as well as that measured by Green (Green and Morgan, 1999) for larger

diameter nano-particles. Remarkably, the data are all consistent with Eq. 4, assuming a surface conductance of 1 nS.

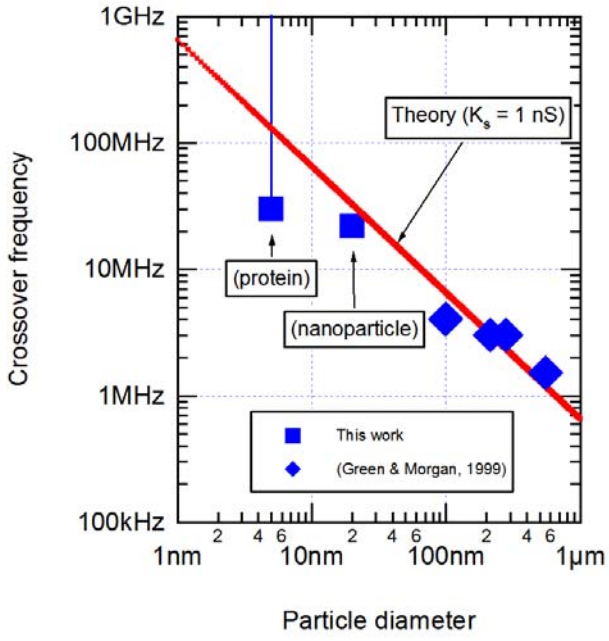

Figure 3.13: Crossover frequency vs. particle diameter in the low suspension conductivity limit. The measurement for the protein crossover frequency corresponds to a lower limit only, limited by the electronics used, thus the bar.

3.9 Discussion: DNA

Unlike proteins, DNA cannot be reasonably modeled as a spherical particle. Under the influence of DEP it is known the DNA is stretched into a long, thin configuration, i.e. it is not randomly coiled. In this section, we provide some elementary discussions of the DEP on DNA, using a simple model for the surface conductivity as we did for the proteins. The failure of this simple model to explain our experimental results indicates that a

fundamental understanding of the mechanism of DEP in manipulating DNA is still lacking.

The polarization factor used in Eq. 1, and hence the Clausius-Mossotti factor given in Eq. 2, are only applicable to spherical particles. In this section we model DNA as an ellipsoid which allows us to use analytical results for the polarization. Based on the induced dipole for an ellipsoid, which can be calculated analytically[95], we define an "effective" Clausius-Mossitti factor, given by[17]:

$$K_{effective}(\omega) \equiv \mathrm{Re}\left(\frac{\varepsilon_p^* - \varepsilon_m^*}{3\left[A\left(\varepsilon_p^* - \varepsilon_m^*\right) + \varepsilon_m^* \right]} \right), \tag{8}$$

where A is the depolarization factor. For an ellipsoid with cylindrical symmetry, it can be shown that A is given by:

$$A = \frac{1-e^2}{2e^3}\left[\log\left(\frac{1+e}{1-e} \right) - 2e \right], \tag{9}$$

where

$$e \equiv \sqrt{1 - \left(\frac{b}{a} \right)^2}, \tag{10}$$

and a and b are the major and minor axis of the ellipsoid.

A question which arises in this context, which has not been addressed to our knowledge, is what effect the charge double layer and the surface conductivity plays in the case of DEP of an ellipsoidal object. O'Konski has provided general arguments (Okonski, 1960) that the induced dipole moment can be calculated using the effective C.M. factor given in Eq. 8, provide the particle conductivity is given by an analog of Eq. 5:

$$\sigma_p = \sigma_b - \frac{2\kappa_s}{b}. \qquad (11)$$

Here b is the minor axis of the ellipsoid.

We now discuss the implications of O'Konski's model in the case of DEP: First, and most importantly, the effective C.M. factor given by Eq. 8 is no longer bound between +1 and -0.5 as is the case with a spherical particle. This is consistent with the well-known polarizability of long, oblate objects. Second, the cross-over from positive to negative DEP is a non-trivial function of the particle geometry and surface conductivity. In order to illustrate this, we have calculated the effective C.M. factor for a reasonable model of stretched DNA: We assume b = 2 nm, a = 18 μm, and K_S = 1 nS. We also assume a medium conductivity of 1 mS/m. Based on this model, we plot in Figure 3.14 the C.M. factor vs. frequency. A crossover frequency from positive to negative DEP is predicted at 6 MHz, and a large polarizability is predicted at low frequencies. In our prediction we did not take into account the Debye length, which is of order 100 nm for low conductivity solutions. If we assume the double-layer has a finite thickness of order 100 nm (by taking b = 100 nm), with surface conductivity still of order 1 nS, the crossover frequency is still of 1 MHz. The crossover frequency is only weekly dependent on the medium conductivity and surface conductivity. To our knowledge, the C.M. factor for an ellipsoid which takes into account O'Konski's prediction for the surface conductivity of the double-layer has not been previously considered.

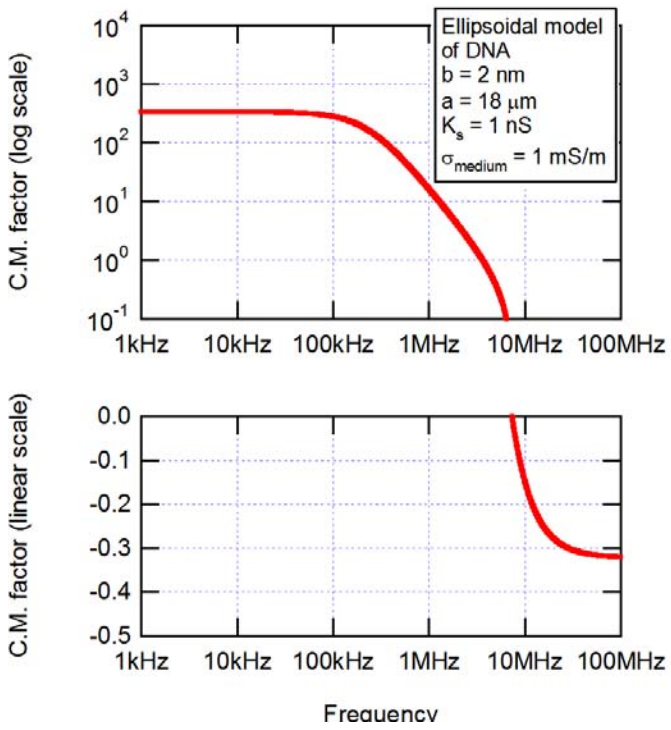

Figure 3.14: Calculated effective C.M. factor for DNA, assuming an ellipsoidal model with a = 2 nm, b = 18 μm, K_s = 1 nS.

The large, low frequency polarizability is consistent with much of the work on DEP manipulation of DNA to date, as discussed in the introductory section. However, the crossover frequency is in disagreement with our experiments, as well as almost all published experiments on DNA. In our experiments show that DNA undergoes positive DEP up to 30 MHz, whereas all previous experiments on DEP of DNA were done below 2 MHz. In this sense our experiments extend the range of data for DEP of DNA by over an order of magnitude in frequency.

In our experiments, the gap between electrodes is less than the stretched length of DNA. Thus, the mathematical treatment of DNA as a simple point-dipole should not be expected to give quantitatively meaningful results; the method of moments in this case should be replaced by a different, perhaps numerical technique. However, this does not

explain the discrepancy with other experiments, for example Washizu's, where the distance between electrodes was much larger than the length of the stretched DNA. We are thus led to conclude that a simple model of DNA as an ellipsoid with an electrical double-layer at the surface described by a surface conductivity simply fails to explain many experimental results, ours included. A fundamental understanding of the molecular basis of DEP manipulation of DNA is still lacking.

3.10 Conclusions

In this work we have described the electronic manipulation of proteins, DNA, and nanoparticles, and applied these for the first time to measure an upper limit on the conductance of DNA and protein molecules that were manipulated with DEP to bridge a gap between electrodes. Our measurements find that DNA and protein is very insulating. Based on former work by Green and Morgan, we have applied a unified description of the double-layer and its effect on the crossover frequency of nanoparticles and proteins, remarkably consistent with previous experiments on DEP manipulation of somewhat larger nanoparticles. Finally, we have pointed out the lack of a fundamental understanding of the DEP manipulation of DNA, and argued that the current model of a simple surface conductivity due to a charge double layer is not consistent with experiment. Looking generally towards the future, our technique for electronically controlled circuit assembly presented herein may be useful for shorter DNA strands or other molecular scale devices, especially when integrated with nanowire and nanotube electrodes[33,51,92].

References

1. Heath, J.R. and Ratner, M.A., *Molecular electronics. Phys. Today* 56, 43–49, 2003.
2. Tour, J.M., *Polym. News* 25, 329–336, 2000.
3. Luo, Y., Collier, C.P., Jeppesen, J.O., Nielsen, K.A., Delonno, E., Ho, G., Perkins, J., Tseng, H.R., Yamamoto, T., Stoddart, J.F. and Heath, J.R., *Chemphyschem* 3, 519, 2002.
4. Braun, E., Eichen, Y., Sivan, U. and Ben-Yoseph, G., *Nature* 391, 775–778, 1998.
5. Winfree, E., Liu, F.R., Wenzler, L.A. and Seeman, N.C., *Nature* 394, 539–544, 1998.
6. Mirkin, C.A., Letsinger, R.L., Mucic, R.C. and Storhoff, J.J. *Nature* 382, 607–609, 1996.
7. Alivisatos, A.P., Johnsson, K.P., Peng, X.G., Wilson, T.E., Loweth, C.J., Bruchez, M.P. and Schultz, P.G., *Nature* 382, 609–611, 1996.
8. Chen, J. and Reed, M.A., *Chem. Phys*. 281, 127–145, 2002.
9. Pethig, R., Biotechnol. 16, 331–348, 1996.
10. Pethig, R. and Markx, G.H., *Trends Biotechnol*. 15, 426–432, 1997.
11. Zimmermann, U., Neil, G.A., Electromanipulation of Cells. CRC Press, Boca Raton, FL, 1996.
12. Ramos, A., Morgan, H., Green, N.G. and Castellanos, A., *J. Phys. D: Appl. Phys*. 31, 2338–2353, 1998.
13. Green, N.G., Ramos, A. and Morgan, H., *J. Phys. D: Appl. Phys. 33*, 632–641, 2000.

14. Hughes, M.P., *Nanotechnology* 11, 124–132, 2000.

15. Burke, P.J., Nano-dielectrophoresis: Electronic Nanotweezers In: Nalwa, H.S. (Ed.), Encyclopedia of Nanoscience and Nanotechnology. American Scientific, Stevenson Ranch, CA, 2004.

16. Pohl, H.A., Dielectrophoresis: The Behavior of Neutral Matter in Nonuniform Electric Fields. Cambridge University Press, Cambridge,1978.

17. Jones, T.B., Electromechanics of Particles. Cambridge University Press, Cambridge, 1995.

18. Morgan, H., Green, N.G., Electrokinetic Technologies for Sub-Micron Particles. Research Studies Press, Philadelphia, PA, 2003.

19. Okonski, C.T., *J. Phys. Chem*. 64, 605–619, 1960.

20. Schwarz, G., *J. Phys. Chem*. 66, p. 2636, 1962.

21. Lyklema, J., Dukhin, S.S. and Shilov, V.N., *J. Electroanal. Chem*. 143, 1–21, 1983.

22. Lyklema, J., Fundamentals of Interface and Colloid Science. Academic Press, San Diego, 2000.

23. Lyklema, J., Springer, M.M., Shilov, V.N. and Dukhin, S.S., *J. Electroanal. Chem.* 198, 19–26, 1986.

24. Green, N.G. and Morgan, H., *J. Phys. D: Appl. Phys*. 30, 2626–2633, 1997.

25. Green, N.G. and Morgan, H., *J. Phys. D: Appl. Phys*. 30, L41–L44, 1997.

26. Green, N.G. and Morgan, H., *J. Phys. D: Appl. Phys. 31*, L25–L30, 1998.

27. Green, N.G. and Morgan, H., *J. Phys. Chem. B* 103, 41–50, 1999.

28. Hughes, M.P., *J. Colloid Interface Sci*. 250, 291–294, 2002.

29. Hughes, M.P., Flynn, M.F. and Morgan, H., *Electrostatics* 163, 81–84, 1999.

30. Hughes, M.P. and Green, N.G., *J. Colloid Interface Sci*. 250, 266–268, 2002.

31. Hughes, M.P. and Morgan, H., *Anal. Chem*. 71, 3441–3445, 1999.

32. Hughes, M.P., Morgan, H. and Flynn, M.F., *J. Colloid Interface Sci*. 220, 454–457, 1999.

33. Zheng, L., Li, S., Burke, P.J., Brody, J.P., *Proceedings of the Third IEEE Conference on Nanotechnology*, 1, 437–440, 2003.

34. Debye, P., Debye, P.P. and Eckstein, B.H., *Phys. Rev*. 94, 1412–1412, 1954.

35. Debye, P., Debye, P.P., Eckstein, B.H., Barber, W.A. and Arquette, G.J., *J. Chem. Phys*. 22, 152–153, 1954.

36. Prock, A. and Mcconkey, G., *J. Chem. Phys*. 32, 224–236, 1960.

37. Losche, A. and Hultschig, H., *Kolloid-Zeitschrift* 141, 177–187, 1955.

38. Eisenstadt, M. and Scheinberg, I.H., *Science* 176, p. 1335, 1972.

39. Eisenstadt, M. and Scheinberg, I.H., *Biopolymers* 12, 2491–2512, 1973.

40. Milner, K.R., Brown, A.P., Allsopp, D.W.E. and Betts, W.B., *Electron. Lett*. 34, 66–68, 1998.

41. Allsopp, D.W.E., Milner, K.R., Brown, A.P. and Betts, W.B., *J. Phys. D: Appl. Phys*. 32, 1066–1074, 1999.

42. Brown, A.P., Milner, K.R., Allsopp, D.W.E. and Betts, W.B., *Electron. Lett*. 34, 1934–1936, 1998.

43. Suehiro, J., Yatsunami, R., Hamada, R. and Hara, M., *J. Phys. D: Appl. Phys*. 32, 2814–2820, 1999.

44. Bezryadin, A. and Dekker, C., *J. Vacuum Sci. Technol*. B 15, 793–799, 1997.

45. Bezryadin, A., Dekker, C. and Schmid, G., *Appl. Phys. Lett*. 71, 1273–1275, 1997.

46. Bezryadin, A., Westervelt, R.M. and Tinkham, M., *Appl. Phys. Lett*. 74, 2699–2701, 1999.

47. Amlani, I., Rawlett, A.M., Nagahara, L.A. and Tsui, R.K., *Appl. Phys. Lett*. 80, 2761–2763, 2002.

48. Porath, D., Bezryadin, A., de Vries, S. and Dekker, C., *Nature* 403, 635–638, 2000.

49. Bhatt, K.H. and Velev, O.D., *Langmuir* 20, 467–476, 2004.

50. Hermanson, K.D., Lumsdon, S.O., Williams, J.P., Kaler, E.W. and Velev, O.D., *Science* 294, 1082–1086, 2001.

51. Zheng, L., Li, S., Burke, P.J., *Proc. of SPIE, 5515, p117*, 2004b.

52. Bezryadin, A.; Dekker, C., *J Vac Sci Technol B* 1997, *15*, 793-799

53. Yamamoto, K., Akita, S. and Nakayama, Y., *Jpn. J. Appl. Phys. Part 2: Lett*. 35, L917–L918, 1996.

54. Yamamoto, K., Akita, S. and Nakayama, Y., *J. Phys. D: Appl. Phys*. 31, L34–L36, 1998.

55. Wakaya, F., Nagai, T. and Gamo, K., *Microelectron. Eng*. 63, 27–31, 2002.

56. Bubke, K., Gnewuch, H., Hempstead, M., Hammer, J. and Green, M.L.H., *Appl. Phys. Lett*. 71, 1906–1908, 1997.

57. Chen, X.Q., Saito, T., Yamada, H. and Matsushige, K., *Appl. Phys. Lett*. 78, 3714–3716, 2001.

58. Diehl, M.R., Yaliraki, S.N., Beckman, R.A., Barahona, M. and Heath, J.R., *Angew. Chem. Int. Ed*. 41, 353, 2001.

59. Nagahara, L.A., Amlani, I., Lewenstein, J. and Tsui, R.K., *Appl. Phys. Lett*. 80, 3826–3828, 2002.

60. Smith, P.A., Nordquist, C.D., Jackson, T.N., Mayer, T.S., Martin, B.R., Mbindyo, J. and Mallouk, T.E., *Appl. Phys. Lett*. 77, 1399–1401, 2000.

61. Duan, X.F., Huang, Y., Cui, Y., Wang, J.F. and Lieber, C.M., *Nature* 409, 66–69, 2001.

62. Lee, S.W. and Bashir, R., *Appl. Phys. Lett*. 83, 3833–3835, 2003.

63. Washizu, M. and Kurosawa, O., *IEEE Trans. Ind. Appl*. 26, 1165–1172, 1990.

64. Washizu, M., Kurosawa, O., Arai, I., Suzuki, S. and Shimamoto, N., *IEEE Trans. Ind. Appl*. 31, 447–456, 1995.

65. Kabata, H., Kurosawa, O., Arai, I., Washizu, M., Margarson, S.A., Glass, R.E. and Shimamoto, N., *Science* 262, 1561–1563, 1993.

66. Shimamoto, N., *J. Biol. Chem*. 274, 15293–15296, 1999.

67. Kabata, H., Okada, W. and Washizu, M. *Jpn. J. Appl. Phys. Part 1: Regul. Pap. Short Notes Rev. Pap*. 39, 7164–7171, 2000.

68. Ueda, M., Iwasaki, H., Kurosawa, O. and Washizu, M., *Jpn. J. Appl. Phys. Part 1: Regul. Pap. Short Notes Rev. Pap*. 38, 2118–2119, 1999.

69. Yamamoto, T., Kurosawa, O., Kabata, H., Shimamoto, N. and Washizu, M., *IEEE Trans. Ind. Appl*. 36, 1010–1017, 2000.

70. Suzuki, S., Yamanashi, T., Tazawa, S., Kurosawa, O. and Washizu, M., *IEEE Trans. Ind. Appl*. 34, 75–83, 1998.

71. Asbury, C.L., Diercks, A.H. and van den Engh, G., *Electrophoresis* 23, 2658–2666, 2002.

72. Asbury, C.L. and van den Engh, G., *Biophys. J*. 74, 1024–1030, 1998.

73. Ueda, M., Yoshikawa, K. and Doi, M., *Polym. J*. 29, 1040–1043, 1997.

74. Ueda, M., Yoshikawa, K. and Doi, M., *Polym. J*. 31, 637–644, 1999.

75. Chou, C.F., Tegenfeldt, J.O., Bakajin, O., Chan, S.S., Cox, E.C., Darnton, N., Duke, T. and Austin, R.H., *Biophys. J*. 83, 2170–2179, 2002.

76. Tsukahara, S., Yamanaka, K., Watarai, H., *Chem. Lett*. 250–251, 2001.

77. Namasivayam, V., Larson, R.G., Burke, D.T. and Burns, M.A., *Anal. Chem*. 74, 3378–3385, 2002.

78. Holzel, R. and Bier, F.F., *IEE Proc. Nanobiotechnol*. 150, 47–53, 2003.

79. Holzel, R., Gajovic-Eichelmann, N. and Bier, F.F., *Biosens. Bioelectron*. 18, 555–564, 2003.

80. Germishuizen, W.A., Walti, C., Wirtz, R., Johnston, M.B., Pepper, M., Davies, A.G. and Middelberg, A.P.J., *Nanotechnology* 14, 896–902, 2003.

81. Germishuizen, W.A., Walti, C., Tosch, P., Wirtz, R., Pepper, M., Davies, A.G. and Middelberg, A.P.J., *IEE Proc. Nanobiotechnol*. 150, 54–58, 2003.

82. Dewarrat, F., Calame, M. and Schonenberger, C. *Single Mol*. 3, 189–193, 2002.

83. de Pablo, P.J., Moreno-Herrero, F., Colchero, J., Herrero, J.G., Herrero, P., Baro, A.M., Ordejon, P., Soler, J.M. and Artacho, E., *Phys. Rev. Lett*. 85, 4992–4995, 2000.

84. Storm, A.J., van Noort, J., de Vries, S. and Dekker, C., *Appl. Phys. Lett*. 79, 3881–3883, 2001.

85. Cai, L.T., Tabata, H. and Kawai, T., *Appl. Phys. Lett*. 77, 3105–3106, 2000.

86. Okahata, Y., Kobayashi, T., Tanaka, K. and Shimomura, M., *J. Am. Chem. Soc*. 120, 6165–6166, 1998.

87. Fink, H.W. and Schonenberger, C. *Nature* 398, 407–410, 1999.

88. Kasumov, A.Y., Kociak, M., Gueron, S., Reulet, B., Volkov, V.T., Klinov, D.V. and Bouchiat, H., *Science* 291, 280–282, 2001.

89. Fan, F.R.F. and Bard, A.J. *Science* 267, 871–874, 1995.

90. Bard, A.J., Faulkner, L.R., Electrochemical Methods: Fundamentals and Applications. Wiley, New York, 2001.

91. Huang, Y. and Pethig, R., *Meas. Sci. Technol*. 2, 1142–1146, 1991.

92. Zheng, L., Li, S., Brody, J.P., Burke, P.J., *Langmuir,* 20(20), 8612-8619, 2004

93. Washizu, M., Shikida, M., Aizawa, S. and Hotani, H. *IEEE Trans. Ind. Appl*. 28, 1194–1202, 1992.

94. Muller, T., Gerardino, A., Schnelle, T., Shirley, S.G., Bordoni, F., DeGasperis, G., Leoni, R. and Fuhr, G., *J. Phys. D: Appl. Phys*. 29, 340–349, 1996.

95. Stratton, J.A., Electromagnetic Theory. McGraw-Hill Book Company Inc., New York, 1941.

CHAPTER 4

MANIPULATING NANOPARTICLES IN SOLUTION WITH ELECTRICALLY CONTACTED NANOTUBES USING DIELECTROPHORESIS

4.1. Introduction

Dielectrophoresis is an electronic analogue[1,2] of optical tweezers[3] based on the same physical principle: an ac electric field induces a dipole moment on an object in solution, which then experiences a force proportional to the gradient of the field intensity. For both types of tweezers, this force must compete with thermal Brownian[4] motion to be effective, which becomes increasingly difficult as the particle size approaches the nanometer scale. Here we show that this restriction can be overcome by using the large electric field gradient in the vicinity of a carbon nanotube to electronically manipulate nanoparticles down to 2 nm in diameter.

The physical principles of self-assembly that give rise to complicated three dimensional structures on the nanometer scale in both biological and synthetic systems have been studied extensively[5, 6]. The forces at work include non-covalent inter and intra-molecular interactions, i.e. hydrogen bonding, Van der Waals, metal-ligand interactions, π-π stacking, and hydrophobic vs. hydrophilic interactions. These bottom-up principles of self-assembly, while efficient and economical, generally are passive, i.e. they are controlled only by macroscopic quantities such as temperature, pH, and solvent

concentration. It would be a distinct advantage if this assembly process could be actively, electronically controlled, especially with nanometer spatial resolution. In this regard, top-down approaches to the manipulation of matter have been successful at the nanometer scale only with AFM/scanned probed technologies, which are difficult to scale to a massively parallel environment, such as that envisioned in the nascent field of molecular electronics.

In a separate, related research theme, the use of electric fields generated by an external voltage source to actively manipulate the locations of nanometer scale objects and large molecules such as DNA and proteins is well known from conventional, established techniques such as gel electrophoresis. Here, the electrodes used are typically macroscopic in size, i.e. many cm. A recent variant on this research theme is the integration of microelectronic fabrication techniques such as photolithography to fabricate electrodes with dimensions on the order of mm or hundreds of micrometers[7, 8]. In these electrophoresis techniques, charged species respond via the coulomb force to dc electric fields. As a result, a limitation of the technique is that neutral species are unaffected and hence cannot be manipulated.

One available technique to electronically manipulate the position of both neutral and charged species in solution is to use ac electric fields, a technique called dielectrophoresis[1]. The physical principles of dielectrophoresis are well-established. If a polarizable object is placed in an electric field, there will be an induced positive charge on one side of the object an induced negative charge (of the same magnitude as the induced positive charge) on the other side of the object. The positive charge will

experience a pulling force; the negative charge will experience a pushing force. However, in a non-uniform field, the electric field will be stronger on one side of the object and weaker on the other side of the object. Hence, the pulling and pushing forces will not cancel, and there will be a net force on the object. This is the dielectrophoresis (DEP) force.

The key physical insight in this work is that we use carbon nanotubes *as the electrode* to generate the electric field gradient; the nanotubes are electrically contacted by lithographically defined metal electrodes, which are far away from the region of interest, so that the fields from the metal electrodes are numerically insignificant compared to the fields generated by the nanotube itself. Since the electric field gradient in the vicinity of a nanotube is large, nanoparticles as small as 2 nm in diameter can be manipulated in spite of the large tendency for random, thermal Brownian motion important for such small particles. This is an order of magnitude smaller than previous nanoparticles that were manipulated with lithographically defined electrodes, and represents the first use of nanotube electrodes in dielectrophoresis. Because this allows an electronic link to the nanometer world, this technology may find applications as a component of massively parallel, actively controlled nano-manufacturing platforms, and generally speaking may provide a bridge between top-down and bottom-up approaches to nanotechnology.

4.2. Theoretical Background

4.2.1 Quantitative Force Predictions

In an electric field $\vec{E}$, a dielectric particle behaves as an effective dipole with (induced) dipole moment $\vec{p}$ proportional to the electric field, i.e.

$$\vec{p} \propto \vec{E} \quad (1)$$

The constant of proportionality depends in general on the geometry of the dielectric particle. In the presence of an electric field gradient, the force on a dipole is given by

$$\vec{F} = \left(\vec{p} \cdot \vec{\nabla}\right)\vec{E} \quad (2)$$

Combining the two equations, and using known results for the relationship between $\vec{p}$ and $\vec{E}$ for a spherical particle of radius r and dielectric constant ε_p, and taking into account the liquid (medium) dielectric constant ε_m, it can be shown that the force acting on a spherical particle (the *dielectrophoresis* force) is given by[1, 9]

$$\vec{F}_{DEP} = 2\pi v \varepsilon_m K(\omega) \vec{\nabla}\left(\vec{E}^2_{RMS}\right) \quad (3)$$

where v is the volume of the particle, $\vec{E}_{RMS}$ the RMS value of the electric field (assuming a sinusoidal time dependence), and K(ω) the real part of what is called the Clausius-Mosotti factor, which is related to the particle dielectric constant ε_p and medium dielectric constant ε_m by

$$K(\omega) \equiv \mathrm{Re}\left[\frac{\varepsilon_p^* - \varepsilon_m^*}{\varepsilon_p^* + 2\varepsilon_m^*}\right] \quad (4)$$

Here the star (*) denotes that the dielectric constant is a complex quantity, and it can be related to the conductivity σ and the angular frequency ω through the standard formula:

$$\varepsilon^* \equiv \varepsilon - i\frac{\sigma}{\omega} \quad (5)$$

When appropriately applied, equation 5 also takes into account surface conductances[10] of the particles and the electrical double layer formed at the interface between the particle and the medium.

4.2.2 Frequency Dependence

For spherical particles, the Clausius-Mosotti factor K(ω) can vary between -0.5 and +1.0. When it is positive, particles move toward higher electric field regions, and this is termed positive dielectrophoresis. When it is negative, the particles move toward smaller electric field regions, and this is termed negative dielectrophoresis. Since K(ω) is frequency dependent, both positive and negative DEP can be observed in the same system by varying the frequency.

4.2.3 Brownian Motion

In addition to DEP forces, small particles also undergo thermal Brownian motion[4]. This can be treated as an effective random force whose maximum value is given roughly by

$$F_{thermal} = k_B T / \sqrt[3]{v} \tag{6}$$

where k_B is the Boltzmann constant, T the temperature, and v the particle volume. In general, there are two regimes of operation for DEP: First, when DEP forces exceed the thermal force. In this case the motion is determined primarily by the DEP force with small, random deviations. In the second case, where the Brownian motion dominates, the particle trajectory is mostly random, with a small tendency to move in the direction of the DEP force. According to equation 3, the DEP force for a spherical particle scales as the radius cubed, whereas according to equation 6 the thermal force scales as the inverse radius. Therefore, for very small particles, the thermal force will dominate. As equation 3 shows, the DEP force depends primarily on the particle size and the gradient of the

electric field intensity. The field gradient is determined by the electrode geometry, which we now discuss; it is the prime focus of our work.

4.2.4 Electrode Geometry

What generates the electric field and, more importantly, the electric field gradient quantified in equation 3? Generally, this is achieved by two metal electrodes with an applied ac voltage. In this case, the order of magnitude of the electric field is set by the applied voltage divided by the spacing between the electrodes. The *gradient* is more sensitive to the details of the electrode geometry.

Historically[1], the use and study of dielectrophoresis was between a sharp pin and a flat surface, because that is the easiest geometry in which one can create a strong field gradient, hence a strong dielectrophoretic force. From this geometry, assuming a 500 micron radius for the tip of the pin, 5,000 V for the applied voltage, and 1 mm for the particle distance from the electrode, Pohl predicted that for particles smaller than 500 nm the DEP force would be negligible compared to Brownian motion[1].

Since the advent of optical and then electron-beam lithography, the use of micro-fabricated planar metal electrodes on insulating substrates has achieved much more attention, since it allows many different flexible geometries to be designed, tested, and used. Moreover, by using small gaps between electrodes, large electric field strengths can be achieved, thus further increasing (in general) the achievable dielectrophoretic force.

The manipulation of spherical nanoparticles down to about 15 nm has been achieved using lithographically defined electrodes, including both metallic and insulating nanoparticles. (A recent review contains exhaustive references to the scholarly literature covering the manipulation of nanoparticles with lithographically defined electrodes[2].)

Nanoparticles smaller than this have not been manipulated because, even with lithographically fabricated electrodes, the field gradients are not large enough to allow the magnitude of the DEP force to overcome thermal motion for nanoparticles smaller than about 15 nm in diameter.

4.2.5 DEP Forces on Prolate Objects

We turn next to the discussion of prolate objects. Equation 3 applies to spherical particles, but it is well known that long, thin objects have enhanced polarizability. For DEP, this means that objects with a few nm diameter that are of order microns in length can still be manipulated by electrical field gradients generated by lithographically fabricated electrodes. Three interesting cases are DNA, nanotubes, and nanowires. Experimentally, it has been possible to align these objects with DEP and then cause them to bridge the gap between two lithographically fabricated electrodes, thus making electrical contact. Although extensive research has been performed on the manipulation of DNA[13], nanotubes[14-25], and nanowires[26-28] using electric fields generated from lithographically fabricated metal electrodes, that is specifically *not* the topic of this work, as we discuss next.

4.2.6 Carbon Nanotubes as Electrodes

All DEP studies to date have used lithographically fabricated metal electrodes to generate the electric field gradients, and therefore have been limited as to the smallest particle size they can manipulate. The key physical insight in this work is that we use carbon nanotubes *as the electrode* to generate the electric field gradient; the nanotubes are

electrically contacted by lithographically defined metal electrodes. Hence, in this work we are able to manipulate nanoparticles with nano-electrodes down to 2 nm in diameter using dielectrophoresis, an order of magnitude smaller than previous nanoparticles that were manipulated. A schematic diagram indicating this principle is shown in Figure 4.1.

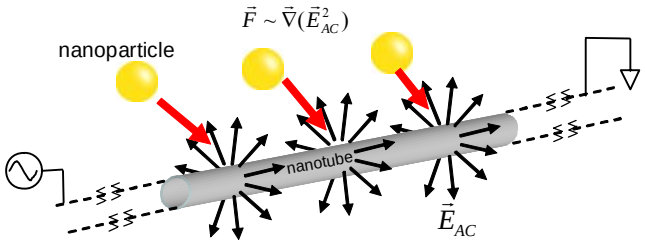

Figure 4.1: Schematic geometry showing the electrically contacted nanotube as the electrode. Except near the ends (which are usually covered by thin film electrodes), the nanoparticles experience an inward radial force towards the surface of the nanotube.

4.3 Experimental Methods

4.3.1 Sample Fabrication.

The carbon nanotubes were grown with chemical vapor deposition from lithographically defined catalyst sites, after Kong[29]. Using conventional photolithography we fabricate wells directly in photoresist (Shipley 1827) on a 4" oxidized (300 nm) silicon wafer (100, n-type, resistivity 5-10 Ω-cm), or onto quartz slides. Next, 2.0 g of alumina nanoparticles (Degussa, aluminum oxide C), 2.5 mmol of $Fe(NO_3)_3 \cdot 9H_2O$ (Aldrich), and 0.7 mmol of $MoO_2(acac)_2$ (Aldrich) are added to 60 ml D.I. water in sequence while violently stirring. Since the $Fe(NO_3)_3$ is soluble in water, spinning this solution directly onto the wafer would remove most of the Fe. This would be an undesirable consequence, since the Fe plays a crucial catalytic role in the nanotube growth. To alleviate this problem, 15 ml of

ammonia (concentrate) was slowly dropped into the mixture above. This caused the formation of $Fe(OH)_3$, which precipitates. The mixture was stirred for 24 hours followed by sonication for 3 hours, resulting in a suspension of 1.25 mmol Fe_2O_3/0.7 mmol MoO_3/2.0 g alumina and water. Two drops of this suspension were deposited onto the patterned photoresist. After spinning on the suspension at 3400 rpm for 40 seconds, and after a 100 C 20 minute bake, lift-off of the photoresist in acetone led to the final sample with catalyst pattern ready to carry out CVD.

CVD was carried out using a 3" Lindberg furnace. A gas recipe that favors the synthesis of ultra-long and high quality SWNTs was adopted in the experiment. After heating up the 3" quartz tube to 900 C under an argon atmosphere, the argon was replaced by a co-flow of 1000 sccm methane (99.999%), and 200 sccm hydrogen for 12 minutes. All the processes were performed under manual control, including purging Ar, increasing the temperature, flowing active gases and cooling down the system in the Ar atmosphere again. After CVD, we find our nanotubes are strongly Van der Waals bound to the surface, and stay that way for the rest of the sample preparation and DEP experiments. To be clear, *in contrast to previous work where metal electrodes were used to manipulate nanotubes freely suspended in solution (see II.5), our nanotubes are firmly bound to the surface and do not move during the entire course of the experiments.*

As-obtained samples were characterized by a scanning electron microscope (SEM) (Hitachi S-4700) using beam energies of 1 keV. Typical nanotube lengths were between 1 and 50 microns in length. AFM images of growth results show that the diameter of as grown nanotubes is less than 1.5 nm. Thus we infer that the nanotubes grown from the nanoparticle catalysts are single walled nanotubes (SWNTs).

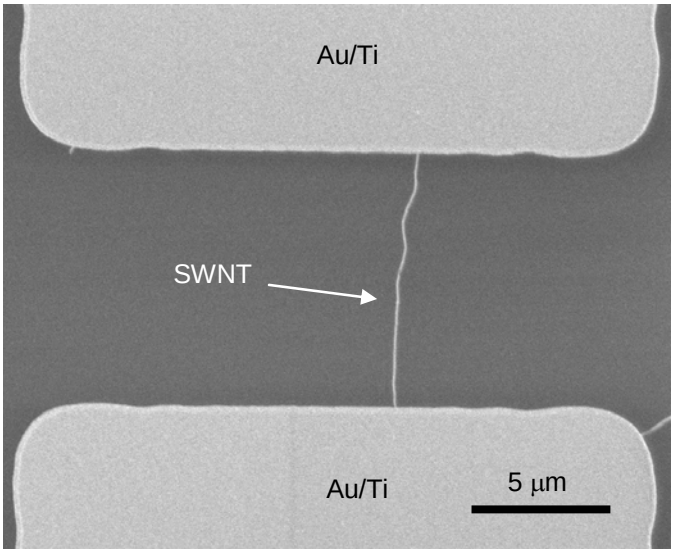

Figure 4.2: SEM image of typical nanotube contacted electrically with Au/Ti bi-layer, before the DEP experiments.

After the location of the nanotubes with respect to the catalyst pads was determined under SEM, optical lithography was used to electrically contact the nanotubes using thermal or electron-beam evaporation of 10nm Ti/100 nm Au and liftoff. The catalyst pads were used as optical alignment marks. The electrode geometry included a 5-10 micron gap between two Au electrodes. Each Au/Ti electrode was electrically contacted with a 25 micron gold wire using bond pads ~ 1 mm^2 located approximately 1 cm away from the gap. Figure 4.2 shows an SEM image of a sample after electrical contact. In some cases, more than one nanotube was contacted on both ends. In other cases, a nanotube would be contacted by one electrode but not the other. Additionally, there were cases where nanotubes were near the electrodes, but not contacted at all. Some typical cases are indicated schematically in Figure 4.3.

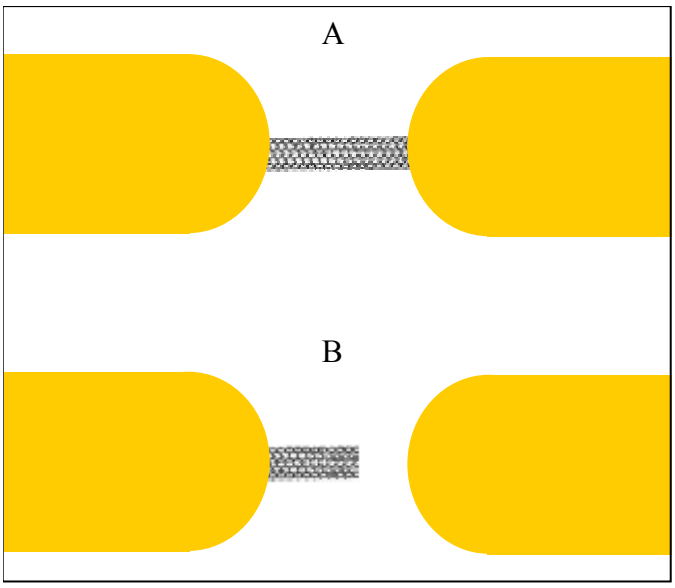

Figure 4.3: Schematic of electrode geometry for studies presented in this work. A) Nanotube electrically contacted on both ends. B) Nanotube electrically contacted on one end only. For this case, the nanotube in may point in a random direction.

4.3.2 Nanoparticle Suspensions

Two types of nanoparticles suspensions were used in this work: Polystyrene nanoparticles of diameters 20 and 100 nm, and Au nanoparticles of diameters 2 and 10 nm. For the polystyrene nanoparticles, suspensions of commercially available (Molecular Probes, Inc.) carboxylate-modified, fluorescently labeled polystyrene nanoparticles (d=20nm or 100 nm) were diluted 10^4 times with D.I. water (18 MΩ-cm) to a density of approximately 10^{11} particles/mL. (The as-purchased nanoparticles were suspended in 2 mM sodium azide; the sodium azide was thus also diluted to 200 nM.) For the Au nanoparticles, suspensions of commercially available (Ted Pella, Inc.) colloidal Au (d=2

nm or 10 nm) were diluted 10^9 times with D.I. water (18 MΩ-cm) to a density of approximately 10^5 particles/mL. No electrolyte was used in either suspension.

4.3.3 Experimental Protocol

In our experiments, electrical connection to the nanotubes is achieved by evaporated Au/Ti electrodes as described in section III.1. Samples were rinsed in methanol and D.I. water before the experiments. Au wires are soldered to the Au/Ti electrodes with In solder, and then connected to a function generator (Stanford Research Systems, model DS 345). An aliquot of suspension (6 μL) is dropped onto the chip containing the electrically contacted single walled carbon nanotubes. The implications of this geometry on the electric field distribution will be discussed in the next section.

Several protocols were tested to see if they were suitable for DEP manipulation. All protocols involved the application of an ac voltage to one gold electrode after dropping the aliquot onto the sample, while the other gold electrode was grounded. The aliquot covered the nanotubes and part of the gold electrodes. In some experiments the sample was allowed to dry in air while the ac voltage was applied. In some experiments, a cover slip was used and the solution was allowed to dry while the ac voltage was applied. In some experiments, the ac voltage was turned off before the solution dried, and a D.I. water rinse was applied, which was then allowed to dry.

An sinusoidal ac voltage is applied at 500 kHz for the polystyrene nanoparticles and 500 kHz -10 MHz for the Au nanoparticles, both with amplitude of 4-20 V_{pp}. The frequency was chosen low enough to be in the positive DEP region, but high enough so the electrolysis would not occur. Prior experiments in our lab on DEP manipulation of

polystyrene nanoparticles using lithographically fabricated gold electrodes found a crossover from positive to negative DEP at 5 MHz for 100 nm nanoparticles, and 20 MHz for 20 nm nanoparticles[13], so that our experiments should be in the positive DEP region. This means the particles will be attracted to regions of highest field intensity. As we discuss below, this is at the surface of the nanotube. During the experiments, the ac current was not measured, but can be estimated. Typical resistances of nanotubes for this work are on the order of 100 $k\Omega - 1\ M\Omega$, so that the current flowing through the nanotube is of order 10 μA. Since the suspending solution was D.I. water, the ac electrical current flowing through the colloidal suspension is assumed to be negligible.

In some experiments where quartz was used as the substrate, the sample was imaged through an inverted Nikon TE200 microscope, equipped with a 20x/1.3NA objective. This was done during the application of the ac voltage. Fluorescent images used epi-illumination with a mercury arc lamp providing the excitation. A Nikon Coolpix 995 camera captured the images.

4.3.4 Post-DEP Characterization Techniques

After DEP manipulations, the samples were characterized in either an SEM (Hitachi S-4700) or an AFM (Digital Instruments, Multimode) in tapping mode. SEM imaging on insulating substrates (such as quartz) can be complicated by substrate charging effects. Therefore, for some samples, a thin layer (10 nm) of Au is sputtered onto the sample to enhance the SEM image contrast.

4.3.5 Electric Field Distribution

Since our nanotubes are several microns long, most nanoparticles will be very far from the ends of the nanotube compared to the size of the nanoparticle and the diameter of the nanotube. For this reason, we focus mainly on the electric field distribution for positions very far from the ends of the nanotubes. In this case, the electric field direction will be primarily radial, as will the direction of the gradient and hence DEP force. Effects of the nanotube ends will be discussed later in this section. Therefore, most nanoparticles experience a predominantly *inward radial force*, independent of the position along the nanotube.

In order to estimate the magnitude of the DEP force, it is necessary to know the electric field distribution, especially the gradient. In this work, we focus on using physical insight and model geometries. This allows estimates of scaling laws and semi-quantitative force calculations. Figure 4.4 shows the geometry of interest. For the purposes of this work we model the nanotube as a metal wire with diameter of 1 nm. While nanotubes are not perfect metals, this approximation is sufficient to approximate the spatial electric field distribution.

The boundary condition at the surface of a metal is that the electric field is perpendicular to the surface. This means the fields at the surface of a nanotube (in our toy model) will point radially. In order to understand from a qualitative perspective the field gradients in the vicinity of a nanotube, we consider Figure 4.4 in more detail. This geometry is appropriate for our experiments performed on oxidized Si wafers. Since the Si wafer is doped, it can be considered a good conductor, hence an equipotential (i.e. a ground plane). The distance from the nanotube to the doped Si is about 300 nm, whereas the

nanotube diameter is about 1 nm. Therefore, we can consider the limit where h >> d. In this case, and when the nanotube length is much larger than h, the radial electric field close to the nanotube is given approximately by:

$$\vec{E}_{RMS} \approx \frac{V_{RMS}}{\ln(4h/d)} \frac{1}{r} \hat{r}, \tag{7}$$

where V_{RMS} is the RMS ac voltage applied to the nanotube, r is the radial distance away from the center of the nanotube, and $\hat{r}$ is a unit vector pointing in the radial direction. From this, we can calculate the gradient of the electric field squared, finding:

$$\vec{\nabla}\left(E_{RMS}^2\right) \approx -2\left(\frac{V_{RMS}}{\ln(4h/d)}\right)^2 \frac{1}{r^3} \hat{r}. \tag{8}$$

The key point of this work is that, because the field gradient and hence DEP force scale as $1/r^3$, and because r can be in the nanometer regime when carbon nanotubes are used as electrodes, the DEP force can overcome Brownian motion even for the smallest of nanoparticles.

Based on this simple calculation, for an applied voltage of 1 V, the DEP force at the surface of the nanotube experienced by a 1 nm dielectric particle (taking r= 0.5 nm, d= 1 nm, h=300 nm) can be estimated using equation 3 as ~ 100 pN, whereas the effective thermal Brownian motion random force for a 1 nm particle from equation 6 can be estimated as ~ 1 pN. This simple calculation, then, predicts that the DEP forces on even the smallest of nanoparticles should be larger than the thermal motion effective force if nanotubes are used as the electrodes.

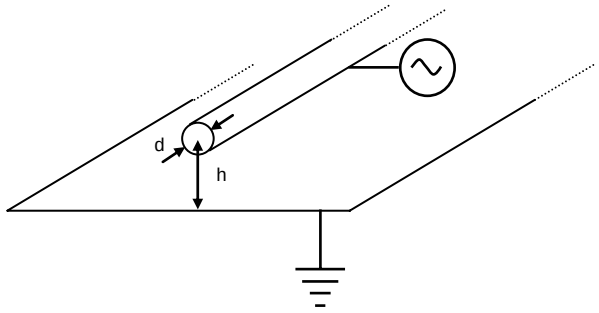

Figure 4.4: Model geometry for cylinder above a ground plane. In practice there is a dielectric (oxide) between the nanotube and the conducting Si substrate.

The above calculations should be taken as estimates only, which use classical electromagnetics to estimate the behavior of electrical nanosystems. For example, for an applied voltage of 1 V on the nanotube, equation 7 predicts an electric field of order 10^7 V/m, which is quite large. Other physical effects probably are important in the nanometer scale, which will cause the real electric field to be less than this value. While these other effects are currently not clearly understood, our work described below demonstrates that the simple physical insight of using nanotubes as electrodes does indeed work experimentally.

For the nanotubes electrically contacted at one end, the ac voltage was applied to the electrode connected to the nanotube. Since very little current flows into the nanotube, the voltage drop along the length of the nanotube is negligible. Therefore, the circuit model shown in Figure 4.4 is valid along the entire length of the nanotube, except near the ends. For nanotubes which are electrically contacted at both ends, since our nanotubes are several microns long, and probably somewhat resistive compared to the gold electrodes, the local voltage between the nanotube and the substrate will vary along the length of the

nanotube. At the nanotube end closest to the grounded gold electrode, the voltage on the nanotube with respect to ground will be zero. On the other hand, at the nanotube end closest to the electrode with the voltage applied, the nanotube – ground plane voltage difference will be largest. Very close to the gold electrodes (on a scale compared to d), the electrical fields will deviated significantly from equation 7. However, for most of the nanotube length in our experiments, equation 7 is a good approximation.

Some of our samples were fabricated on a quartz wafer, which can be considered insulating, so that Figure 4.4 is not appropriate. In that case, the electric field distribution is not as simple to calculate. However, it is still the case that, near the surface of the nanotube, the electrical field is perpendicular to the nanotube, and that the gradient (hence DEP) force should be very large. Our experiments bear out this claim.

There will also be large gradients near the ends of the tubes, which will cause DEP forces there, as well. The very tip of the nanotube will have strong field gradients as well, and similar arguments could be given that the tips could be used to trap nanoparticles. At least one end of the nanotubes in our work are usually covered with Au thin films, but in cases where an end is exposed, we do see trapping of nanoparticles both at the ends and along the length of the nanotubes.

4.4 Results and Discussions

4.4.1 Polystyrene Nanoparticles

26 separate experiments were performed on DEP manipulation of Polystyrene nanoparticles, of which about 25% of them showed clearly attached polystyrene nanoparticles under SEM characterization after drying. We found experimentally that the

nanoparticles are present under SEM independent of whether the cover slip was on or off during drying. Additionally, the results were independent of whether a post-DEP rinse in D.I. water was performed. The results were also independent of the substrate used, showing similar results on both quartz and oxidized Si wafers. In addition, in control experiments where no ac voltage was applied, we never observed the attachment of nanoparticles to nanotubes. Taken collectively, these results lead us to conclude that the ac electric fields are indeed causing the nanoparticles to come into intimate contact with the nanotubes, and that they remain attached to the nanotubes even after D.I. water rinse, solution drying, and exposure to the vacuum environment of an SEM.

In Figure 4.5, we show an SEM image of a nanotube on a quartz wafer both before and after the DEP experiment. This is an example of a nanotube contacted electrically on both ends. The trapped 100 nm nanoparticles are clearly visible preferentially attached along the length of the nanotube, forming a "pearl chain." To allow clearer SEM images, Au was sputtered uniformly onto the entire sample (including the electrodes, nanotube, and attached nanoparticles), and imaged more carefully under SEM. This image is shown in Figure 4.6.

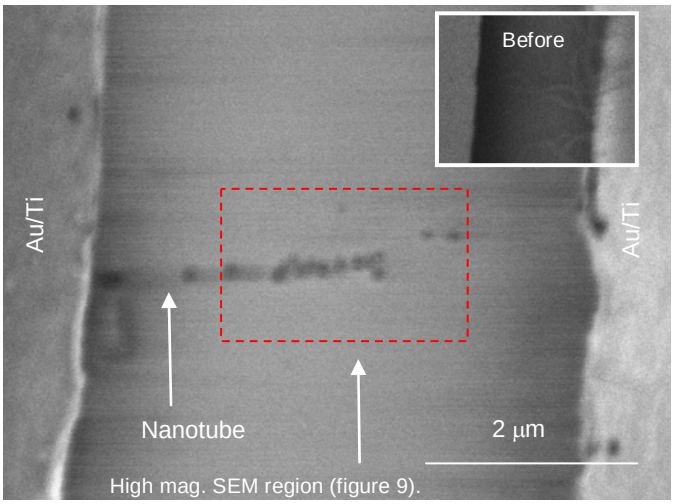

Figure 4.5 SEM images of nanotube contacted electrically on both ends, before and after the trapping experiments using 100 nm polystyrene nanoparticles. The alignment along the tubes is clear.

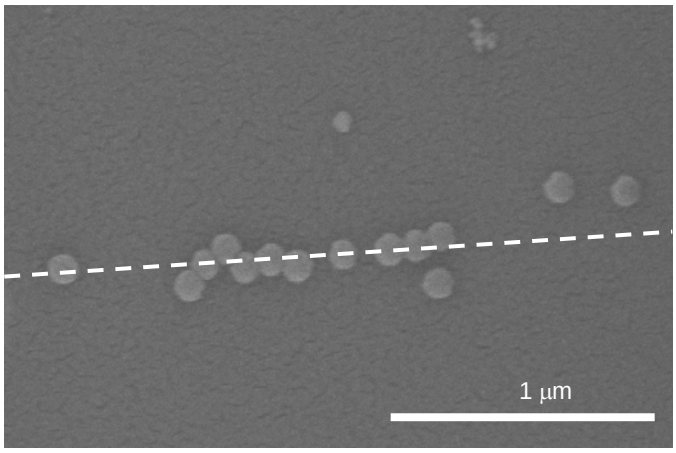

Figure 4.6: High magnification image of region outlined in Figure 4.5, after Au has been sputtered to enhance resolution and contrast of the 100 nm nanoparticles. The dashed white line shows where the nanotube is, which is not visible because it is covered by 10 nm of sputtered Au.

In some experiments, the nanotube was electrically contacted on one end only. In this case, we were also clearly able to see preferential attachment of the nanoparticles to the nanotube. In Figure 4.7, we show a series of images indicating the process. Fig 7a shows an image of the nanotubes and gold electrodes before the DEP experiments. Figure 4.7b shows fluorescence microscopy images taken during the DEP experiment. It clearly shows that the nanoparticles were attached to the nanotubes during the DEP experiment before the solution dried. (In this experiment, both 20 nm and 100 nm nanoparticles were used.) Figure 4.7c shows an SEM image, which indicates the nanoparticles are still attached to the nanotubes, even after the solution dries. In order to more clearly see this, we show in figures 4.8, 4.9 higher magnification SEM images of the nanotube from Figure 4.10c, after sputtering Au onto the whole sample to increase the contrast. The attachment of the nanoparticles to the nanotube is clear.

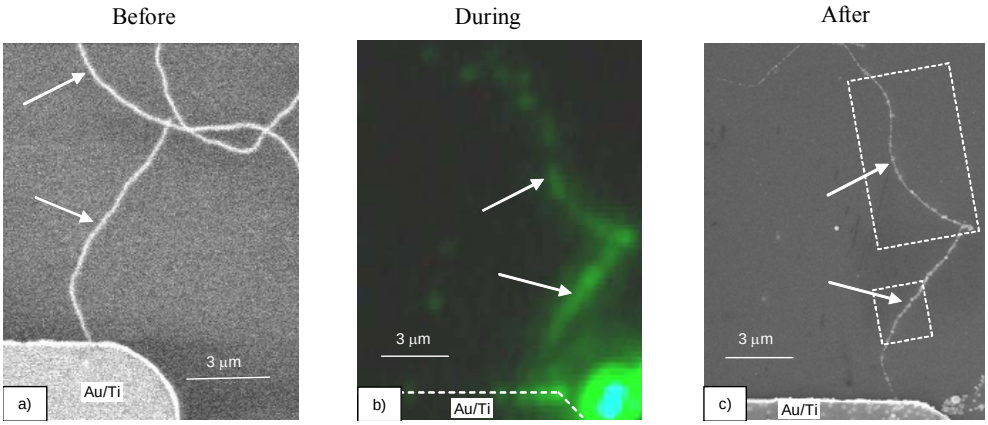

Figure 4.7: Key result of this work. A) SEM image of the nanotubes and gold electrodes before the DEP experiments. B) Fluorescence microscopy images taken during the DEP experiment. (The solution was still on the sample.) C) SEM image of the nanoparticles attached to the nanotubes after the DEP experiments.

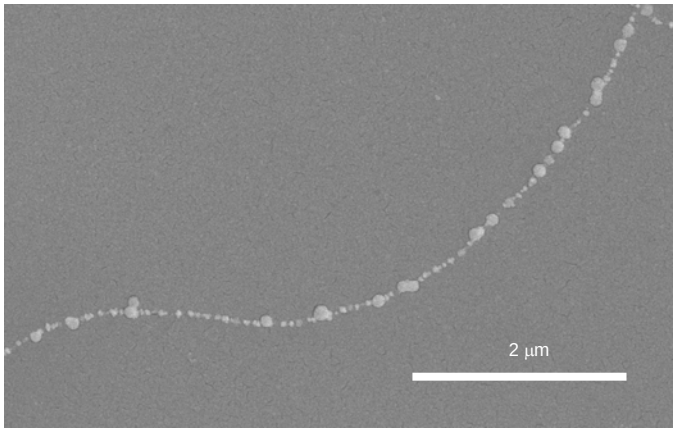

Figure 4.8: Zoom of fig. 4.7.

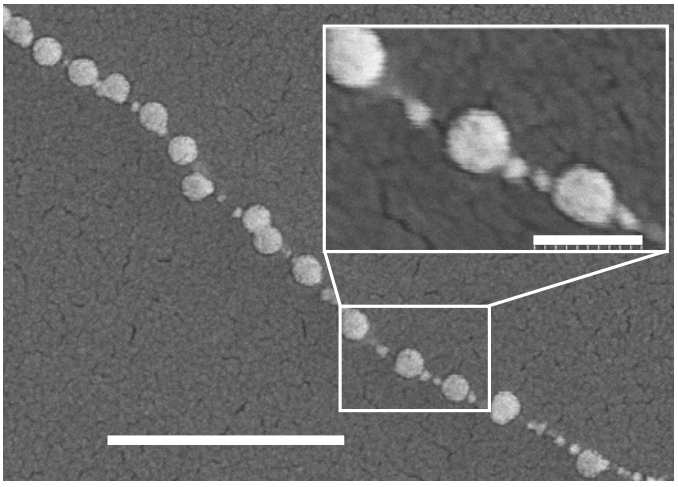

Figure 4.8: Another zoom of fig. 7. Both the 20 nm and 100 nm particles are clearly visible along the length of the nanotube. Scale bar: 1 μm; inset: 200 nm.

4.4.2 Control Experiments and Capillary Forces

Several groups have recently investigated the role of capillary forces in self-assembly. Since the drying force of droplets can be used to make particle chains by self-assembly of microparticles and nanoparticles in groves[30-36] (which is qualitatively different than our

experiments which have no such groves), we have investigated the possibility that capillary forces are at play in our experiments.

Several control experiments were performed to determine the role of capillary forces. First, as discussed above, experiments where no voltage was applied to the nanotubes never resulted in any preferential attachment of nanoparticles to the nanotubes. Figure 4.10 shows a typical SEM image of a control experiment where no ac voltage was applied. Nanoparticles and nanotubes are both clearly visible, and not attached.

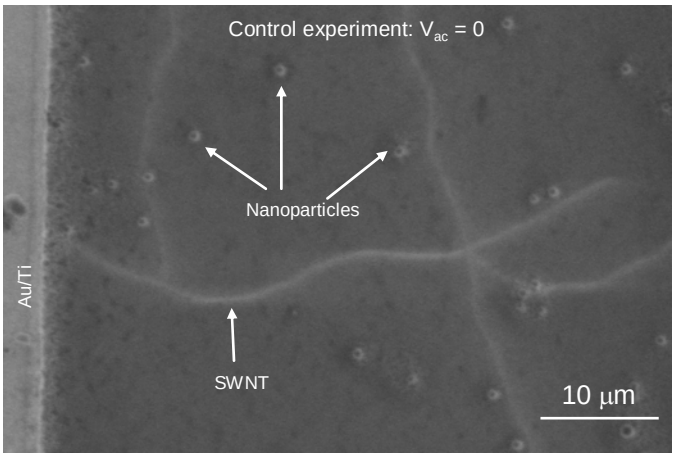

Figure 4.9: Control experiment in which no ac voltage was applied shows that nanoparticles do not attach to nanotubes.

A separate indication that capillary forces are not responsible for the pearl chaining we observe comes from imaging of the fluorescently labeled nanoparticles performed during the application of the ac voltage, before the solution was allowed to dry. While the nanotubes are too small to be visible under an optical microscope, the electrodes were easy to see. Additionally, prior to the experiments, the location of the nanotubes was

determined by SEM. Clear evidence for preferential attachment of the nanoparticles to the nanotube was clearly seen under fluorescence microscopy (see Figure 4.7).

Not all the nanoparticles in the solution are trapped at the surface of the nanotubes. In order to further investigate this issue, we performed control experiments by dropping a small aliquot on the corner of a sample, allowing it to dry, and characterizing the distribution of polystyrene nanoparticles after drying with SEM. We find the dominant population of polystyrene nanoparticles is at the edge of the aliquot that dried. This is due to capillary forces and surface tension moving the nanoparticles as the aliquot dries. However, the population of polystyrene nanoparticles in the original center of the aliquot was low (typically less than 100 nanoparticles per 100 x 100 micron field of view of the SEM). This is similar to what happens to drops of coffee after drying on a table: Rings of dark regions are visible around the edges of the original drop[37]. Thus, since the polystyrene nanoparticle population in the center of the aliquot was not enhanced due to capillary forces after drying, and since the DEP experiments were performed with nanotubes in the center of the original aliquot, we are lead to conclude that many of the nanoparticles that are not attached to the nanotube end up at the edge of the aliquot, which is far (several mm) away from the nanotube.

Taken collectively these control experiments lead us to conclude that capillary forces, while significant, are not responsible for the attachment of the nanoparticles to the nanotubes observed under SEM.

4.4.3 Gold Nanoparticles.

In order to test the scalability of the technique to smaller nanoparticles, we performed similar experiments with 2 and 10 nm Au nanoparticles. In Figure 4.11, we show an SEM image of electrically contacted nanotubes before and after the DEP experiments, where we used a sine wave at 1 MHz, amplitude 2 V_{pp}, and 2 nm Au nanoparticles. In this experiment, there are nanotubes contacted on both ends, as well as nanotubes contacted on only one end. Both types showed attached Au nanoparticles after the DEP experiments under SEM characterization. In two control experiments, an aliquot of Au nanoparticle solution was allowed to dry on a chip where no ac voltage was applied. In those experiments, we found no evidence that nanoparticles bind to the nanotube. Au nanoparticles of d=2 nm were trapped in 6/8 experiments with frequencies form 500 kHz to 10 MHz. Thus, the Au nanoparticle attachment to the nanotube is clearly controlled by the application of an ac voltage.

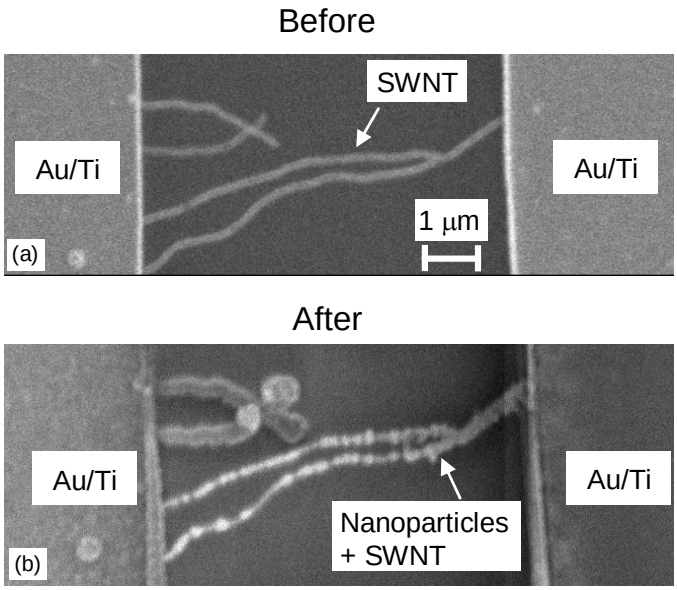

Figure 4.10. SEM image of nanotube contacted electrically on both ends before and after DEP experiments using 2 nm gold nanoparticles. The Au nanoparticles are attached to the nanotubes after the DEP experiments.

A more dramatic example of this Au nanoparticle trapping is shown in Figure 4.12. There, it is clear that the Au nanoparticles are dominantly attracted to the nanotubes. In addition, the gold nanoparticles form on the nanotubes regardless of whether they are straight or curled, whether they have kinks, or even where two nanotubes cross.

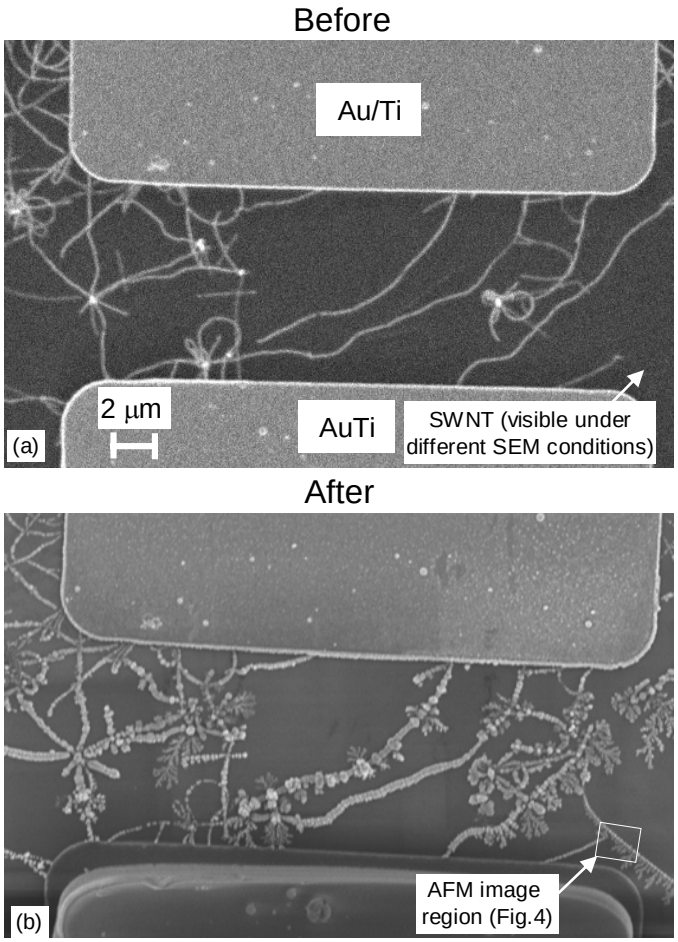

Figure 4.11: SEM images of SWNTs before and after DEP experiments.

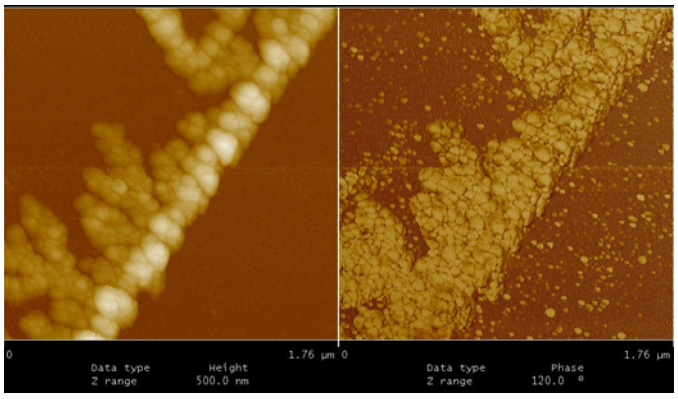

Figure 4.12: A) Tapping mode and b) phase contrast mode AFM images of a Au nanoparticles on a nanotube.

In Figure 4.12, it is interesting to note that a nanotube with Au nanoparticles is visible in the lower-right region of the image where there was no nanotube visible (via SEM) before. Under different SEM conditions, we indeed observe a nanotube where the nanoparticles were trapped. This is consistent with the work of Fuhrer[38], who has clearly shown that SEM images of SWNTs are related closely to the detailed imaging conditions. In order to more closely examine the morphology of the Au particles on the nanotubes, we present in Figure 4.13 an AFM image from a short section of one or our Au nanoparticle nanotubes. The tapping mode image (Figure 4.13a) clearly confirms dendritic growth off the side of some of the nanotubes. Similar dendritic growth has been studied by Velev[39, 40] in complimentary experiments using mm scale electrodes. The phase contrast image (Figure 4.13b) is more difficult to interpret physically, but seems to indicate that if there are any nanoparticles that are not attached to the nanotube, the fraction is small.

4.4.4 Discussion.

In our experiments, we have clearly shown using a variety of techniques and control experiments that the application of an ac voltage to an electrically contacted nanotube in solution causes polystyrene nanoparticles (20 and 100 nm) and Au nanoparticles (2 and 10 nm) to be attached to the nanotubes. This attachment is strong enough to survive the capillary forces present on drying of the solution. We have demonstrated that the attachment of the nanoparticles is not a passive self-assembly process, but rather an active, electronically controlled process.

At present, we do not know the type of bond that occurs at the attachment site. This is clearly a topic worthy of future study. An additional topic which we have not studied includes the effect of the nanotube electrical resistance and crystallographic properties. For example, do semiconducting and metallic nanotubes both give similar results when DEP trapping?

Finally, because the dielectric properties of the nanoparticles are frequency dependent, by varying the frequency, it should be possible to attract or repel nanoparticles; by using different species of nanoparticles, one could attract one species while repelling others. Multiple layers of shells could thus be built up on top of the nanotube. This is just one example of how this technique could be used for electronically controlled assembly of matter at the nanometer scale.

4.5 Conclusions

We have demonstrated, for the first time, the use of nanotube electrodes to manipulate nanoparticles in solution using dielectrophoresis. The technique should find broad applicability. In contrast to AFM based nano-fabrication techniques, this is purely electronic and hence requires no mechanical motion at either the nano-scale[41] or macro-scale. Thus, the technique is inherently scalable for massively parallel nano-manipulation. In addition, it should be possible to manipulate biological nanostructures such as DNA[13], viruses[42] and proteins[43] using nanotube electrodes.

References

1. Pohl, H. A., *Dielectrophoresis : The Behavior of Neutral Matter in Nonuniform Electric Fields*. ed.; Cambridge University Press: Cambridge ; New York, 1978.
2. Burke, P. J., Nanodielectrophoresis: Electronic Nanotweezers. In *Encyclopedia of Nanoscience and Nanotechnology*, ed.; Nalwa, H. S., American Scientific: Stevenson Ranch, CA, 2004.
3. Ashkin, A.; Dziedzic, J. M.; Bjorkholm, J. E.; Chu, S., *Opt Lett* 1986, *11*, 288-290.
4. Einstein, A., *Annalen der Physik* 1905, *17*, 549-560.
5. Whitesides, G. M.; Mathias, J. P.; Seto, C. T., *Science* 1991, *254*, 1312-1319.
6. Philp, D.; Stoddart, J. F., *Angewandte Chemie-International Edition in English* 1996, *35*, 1155-1196.
7. Cheng, J.; Sheldon, E. L.; Wu, L.; Uribe, A.; Gerrue, L. O.; Carrino, J.; Heller, M. J.; O'Connell, J. P., *Nat Biotechnol* 1998, *16*, 541-546.
8. Huang, Y.; Ewalt, K. L.; Tirado, M.; Haigis, T. R.; Forster, A.; Ackley, D.; Heller, M. J.; O'Connell, J. P.; Krihak, M., *Anal Chem* 2001, *73*, 1549-1559.
9. Jones, T. B., *Electromechanics of particles*. ed.; Cambridge University Press: Cambridge ; New York, 1995.
10. Morgan, H.; Green, N. G., *AC electrokinetics : colloids and nanoparticles*. ed.; Research Studies Press, Ltd.: Baldock, Hertfordshire, England, 2003.
11. Wang, X. J.; Wang, X. B.; Becker, F. F.; Gascoyne, P. R. C., *J Phys D Appl Phys* 1996, *29*, 1649-1660.
12. Clague, D. S.; Wheeler, E. K., *Phys Rev E* 2001, *6402*, art. no.-026605.

13. Zheng, L.; Brody, J. P.; Burke, P. J., *Biosens Bioelectron* 2004, 20, 606

14. Bezryadin, A.; Dekker, C., *J Vac Sci Technol B* 1997, *15*, 793-799.

15. Yamamoto, K.; Akita, S.; Nakayama, Y., *Jpn J Appl Phys 2* 1996, *35*, L917-L918.

16. Wakaya, F.; Nagai, T.; Gamo, K., *Microelectron Eng* 2002, *63*, 27-31.

17. Chen, X. Q.; Saito, T.; Yamada, H.; Matsushige, K., *Appl Phys Lett* 2001, *78*, 3714-3716.

18. Yamamoto, K.; Akita, S.; Nakayama, Y., *J Phys D Appl Phys* 1998, *31*, L34-L36.

19. Bubke, K.; Gnewuch, H.; Hempstead, M.; Hammer, J.; Green, M. L. H., *Appl Phys Lett* 1997, *71*, 1906-1908.

20. Krupke, R.; Hennrich, F.; Weber, H. B.; Kappes, M. M.; von Lohneysen, H.,

21. Krupke, R.; Hennrich, F.; Weber, H. B.; Beckmann, D.; Hampe, O.; Malik, S.; Kappes, M. M.; Lohneysen, H. V., *Appl Phys a-Mater* 2003, *76*, 397-400.

22. Nagahara, L. A.; Amlani, I.; Lewenstein, J.; Tsui, R. K., *Appl Phys Lett* 2002, *80*, 3826-3828.

23. Chung, J. H.; Lee, K. H.; Lee, J. H., *Nano Lett* 2003, *3*, 1029-1031.

24. Kumar, M. S.; Lee, S. H.; Kim, T. Y.; Kim, T. H.; Song, S. M.; Yang, J. W.; Nahm, K. S.; Suh, E. K., *Solid State Electron* 2003, *47*, 2075-2080.

25. Chung, J. Y.; Lee, K. H.; Lee, J. H.; Ruoff, R. S., *Langmuir* 2004, *20*, 3011-3017.

26. van der Zande, B. M. I.; Koper, G. J. M.; Lekkerkerker, H. N. W., *J Phys Chem B* 1999, *103*, 5754-5760.

27. Smith, P. A.; Nordquist, C. D.; Jackson, T. N.; Mayer, T. S.; Martin, B. R.; Mbindyo, J.; Mallouk, T. E., *Appl Phys Lett* 2000, *77*, 1399-1401.

28. Huang, Y.; Duan, X. F.; Wei, Q. Q.; Lieber, C. M., *Science* 2001, *291*, 630-633.

29. Kong, J.; Soh, H. T.; Cassell, A. M.; Quate, C. F.; Dai, H. J., *Nature* 1998, *395*, 878-881.

30. Xia, Y. N.; Yin, Y. D.; Lu, Y.; McLellan, J., *Adv Funct Mater* 2003, *13*, 907-918.

31. Yin, Y. D.; Lu, Y.; Gates, B.; Xia, Y. N., *J Am Chem Soc* 2001, *123*, 8718-8729.

32. Yin, Y. D.; Xia, Y. N., *Adv Mater* 2001, *13*, 267-271.

33. Yin, Y. D.; Xia, Y. N., *J Am Chem Soc* 2003, *125*, 2048-2049.

34. Yin, Y. D.; Lu, Y.; Xia, Y. N., *J Mater Chem* 2001, *11*, 987-989.

35. Gates, B.; Yin, Y. D.; Xia, Y. N., *J Am Chem Soc* 2000, *122*, 12582-12583.

36. Lu, Y.; Yin, Y. D.; Xia, Y. N., *Adv Mater* 2001, *13*, 271-274.

37. Deegan, R. D.; Bakajin, O.; Dupont, T. F.; Huber, G.; Nagel, S. R.; Witten, T. A., *Nature* 1997, *389*, 827-829.

38. Brintlinger, T.; Chen, Y. F.; Durkop, T.; Cobas, E.; Fuhrer, M. S.; Barry, J. D.; Melngailis, J., *Appl Phys Lett* 2002, *81*, 2454-2456.

39. Bhatt, K. H.; Velev, O. D., *Langmuir* 2004, *20*, 467-476.

40. Hermanson, K. D.; Lumsdon, S. O.; Williams, J. P.; Kaler, E. W.; Velev, O. D., *Science* 2001, *294*, 1082-1086.

41. Kim, P.; Lieber, C. M., *Science* 1999, *286*, 2148-2150.

42. Morgan, H.; Hughes, M. P.; Green, N. G., *Biophys J* 1999, *77*, 516-525.

43. Washizu, M.; Suzuki, S.; Kurosawa, O.; Nishizaka, T.; Shinohara, T., *Ieee T Ind Appl* 1994, *30*, 835-843.

CHATER 5

PROBING NANOTUBE-PEPTIDE INTERACTIONS ON A SILICON CHIP USING MOLECULAR BIOLOGY TOOLS

5.1. Introduction

Using the tools of modern molecular biology, we probe the interaction of nanotubes on silicon chips with proteins via combinatorial phage display methods. In our work we have found a tryptophan rich binding motif to SWNTs on a solid silicon substrate. The motif resembles and alpha helix with tryptophan concentrated along one side that binds non-covalently via pi-pi interactions to the walls of the nanotube.

What is the nature of the interaction between nanotubes and proteins and peptides? Peptides can act as surfactants to solubilize nanotubes in aqueous solutions. Peptides which bind with specificity to different nanotube allotropes (specific to the n,m index) may allow for economical nanotube-sorting and purification technologies. Eventually, one may be able to engineer self-assembled, controllable placement and location control of nanotube devices with nm precision using protein self-assembly analogous to so-called DNA nanotechnology. Finally, the development and understanding of nanotube interaction with living systems at the cellular level is significant for potential therapeutic and/or cytotoxic effects[1-3]. However, to date a thorough understanding at the molecular level of nanotube-protein interactions is still lacking, and the understanding of nanotube-peptide interactions can be considered the first and most fundamental step in understanding this complex system.

The hydrophobic nature of SWNTs is by now well known, and prevents their solubility in aqueous solutions without the presence of surfactants. Thus, the study of surfactants[4] has been an important research theme, and has led to clear understanding that π- π interaction can cause hydrophobic side groups of surfactants (anionic, cationic, and various polymer surfactants) to bind non-covalently to SWNTs. DNA and some peptides also contain aromatic side groups which can bind to the SWNTs and thus act to solubilize SWNTs. While the ability of DNA to bind differently to semiconducting and metallic SWNTs has been demonstrated[6], the binding of proteins or peptides to nanotubes of differing electronic properties has not been demonstrated. Because of the importance of aromaticity on SWNT binding[7], the three aromatic amino acids Phenylalanine (Phe), Tyrosine (Tyr), and Tryptophan (Trp) have been the focus of most studies to date.

Dieckman et al designed, synthesized, and demonstrated a SWNT binding amphiphilic alpha helix using Phe side groups distributed along one side of the helix[8]. Because of the amphiphilic nature of the peptides, conglomeration of the nanotube/peptide system occurred at high salt concentrations, when the ions shielded the electrostatic charges on the amphiphilic helices which prevent conglomeration at low ionic strength. Wang et al[9] studied binding to MWNTs using phage display (PD) techniques, and found binding sequences which consisted of "symmetric surfactants": hydrophilic on the ends, and hydrophobic in the middle. In addition, His and Trp are found to have important roles, but not Phe. Pender & Honek[10, 11] studied SWNTs with PD and found that His and Trp are important among binding peptides. The role of Trp was further probed by Honek[12] using artificial analogs of Trp and studying their effect on binding to SWNTs. Very recently Dalton et al studied the relative binding of Trp, Phe, & Tyr to SWNTs using

amino acids on the end of a surfactant peptide[13]. They found that Trp bound stronger than Phe or Tyr. Additional studies[14] by the same group have elucidated the role of peptide-nanotube interactions where Phe side groups (as well as artificial analog nitro-phenylalanine and tyrosine) are along an alpha-helix. Using cell surface display[15] (rather than PD), Brown found that His and also a large number of aromatic AAs are not required (only 1 is required) for SWNTs on Si wafers.

In all the above phage display experiments, carbon nanotubes were suspended in the solution. This method, however, inevitably raised a problem of nanotube bundles: either difficulties in separating as-grown nanotube bundles into individual ones although an ultrasonic method might help to a certain degree; or causing individual nanotubes bundling together in solution, especially during the incubation process where a step of gentle rocking is involved. The bundles can cause the redistribution of energy levels of the individual ones, which might destroy the binding affinity of phage virons on the individual nanotubes. Another problem was also caused since tween was used in these experiments. Tween, used in the experiments of the traditional targets like protein or other inorganic targets like gold and silicon materials, is for removal of the nonspecifically bound phage. However, for the carbon nanotubes, the interaction between nanotubes and phage is mainly hydrophobic while tween, a detergent known for the disruption of hydrophobic interactions, will play an opposite role if used. We discuss it in detail later.

In this work, we also use phage display to find peptides which bind to SWNTs. However, in contrast to prior work, our SWNTs were CVD grown on and thus tightly bound to solid (SiO_2) substrates. Such nanotubes grown on the substrate are mainly individual

ones. Therefore the bundle problem can be solved. Another advantage of using nanotubes grown on solid substrates is that the centrifugation steps in the wash and elution processes can be avoided and thus that there are no bound nanotubes removed during these steps.

We also develop a new elution buffer and demonstrate that it is more appropriate and efficient for elution of hydrophobic binders. This paves a way for the phage display experiments of a single but long nanotube where the efficiency of elution is required. Here, it is worthy to mention the importance of such kind of experiments: a nanotube with a specific (n,m) index might correspond to a specific motif of a bound phage; therefore, the recognition of specific nanotubes can be realized by carrying the phage display experiment and sequencing the DNA of the bound phage.

We find a qualitatively new binding sequence which is distinct from prior binding sequences found by PD. The binding sequence we find consists of Trp side groups distributed along one side of the peptide, similar to that designed from first principles by Dalton using Phe side groups. We speculate the reason that prior experiments did not find this binding sequence is that the SWNTs in prior PD experiments were in solution, whereas in our experiments they are van der Waals bound to the substrate, and also because we have developed a new for nanotube elution buffer more appropriate for the hydrophobic nature of the nanotube-peptide interaction. The new motif is a non-surfactant, nanotube-binding peptide.

5.2. Results & Discussion

In our experiments, we used SWNTs on silicon wafers grown in place using CVD, using recipes as described in[16, 17]. A combinatorial library of peptides expressed on this surface of a phage virus to screen for peptides with specific affinity for SWNTs, as shown in Figure 1. The nanotubes are strongly bound to but not seamlessly cover the substrate, and hence a key challenge was to determine peptide interaction with the substrate as opposed to the nanotubes.

5.2.1. Motifs found

The goal of the experimental trials was to find a binding sequence that binds specifically to nanotubes (not the substrate). Convincing evidence for this would require two observations: First, the titer should gradually increase with increasing panning rounds. This would be due to continual enrichment of nanotube binding motifs in the pool of virions. Second, the control experiment (wafers with no nanotubes) should have a qualitatively different consensus motif of sequence than the nanotube sample.

A variety of buffers were used for washing and elution. We found that TBS with 0.5% (v/v) tween (TBST 0.5) acts as a very effective elution buffer, much more effective than the standard glycine-HCl (Gly-HCl). This is different than prior nanotube PD experiments, and we explain how we came to the conclusion and hypothesize why it may be true below.

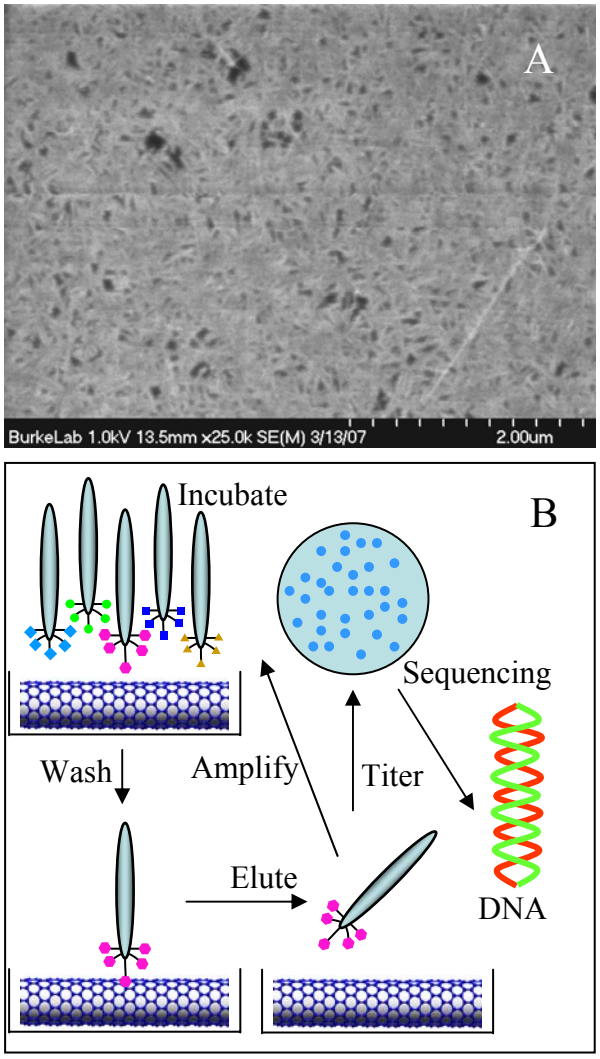

Figure 5.1 SEM images of SWNT networks on SiO2/Si wafer (A) and schematic phage display procedure (B).

Using TBST as the elution buffer allowed us to observe completely different motifs between nanotube coated wafers and control wafers with no nanotubes. 16 of 19 sequences obtained from two SWNT samples are rich in tryptophan. The sequences are shown in Table 5.1. Among them, 11 sequences showed a motif of SXWWXXW. Tryptophan is nonpolar and very hydrophobic amino acid with an indole function group on the side chain, which can stack along the surface of carbon nanotubes. On the other

hand, there are only 4 counts of histidine in the total 228 amino acids in the nanotube samples, which is only a quarter of the observed frequency in the NEB library.

No.	Amino acids												Occurrence
1	G	**W**	D	**W**	A	Q	D	**W**	N	**W**	**W**	T	1
2	**W**	F	P	I	A	**W**	P	E	S	**W**	Y	H	1
3	Y	T	**S**	P	**W**	**W**	L	A	**W**	Y	D	P	2
4	Y	E	Y	P	**W**	A	N	**W**	**W**	L	S	P	1
5	D	D	**W**	**S**	H	**W**	**W**	R	A	**W**	N	G	3
6	S	**S**	A	**W**	**W**	S	Y	**W**	P	P	V	A	6
7	A	**W**	**W**	E	A	F	I	P	N	S	I	T	1
8	N	D	N	P	**W**	L	M	**W**	L	K	N	**W**	1

Table 5.1. Sequences of peptides bound to single-walled carbon nanotubes. Aromatic amino acids are highlighted in yellow; nonpolar in purple; polar noncharged in blue; polar charged in green.

Thus, we conclude that the Trp-rich binding sequences are specific to the nanotube binding, since under this same set of buffer conditions, the control sequences on wafers with no nanotubes were qualitatively distinct. Further evidence to support this conclusion based on titers and hydrophobicity measurements of the nanotube and control measurements is presented next.

5.2.2. Buffer efficiency

We have conducted a set of experiments to analyze the efficiency of two different potential elution buffers. Two single-walled carbon nanotube (SWNT) samples A and B

(SWNT CVD grown on 1x1 cm^2 SiO_2 wafers) were both incubated for 45 minutes in the TBS solution containing 4 µl Ph.D-12 phage from the random library and unbound phage were washed away with TBS 5 times. Sample A was first eluted with 0.2 M Gly-HCl (pH 2.2) and washed with TBS twice and then eluted with TBST 0.5. Sample B was first eluted with TBST 0.5 and washed with TBS twice and then eluted with Gly-HCl. All four eluants were titered. The titration results of 10 µl 100X dilutions are shown in Table 5.2.

Sample	Elution buffer	Titer (# blue plaques)
A	First Glycine-HCl	19
	then TBST 0.5	>1000
B	First TBST 0.5	>1000
	then Glycine-HCl	72

Table 5.2. Titration results of 10 µl 100X dilutions of four eluants of sample A and B after eluated twice with the different order of two elution buffers. Washing solution was TBS.

Based on the results shown in Table 5.2, we found that TBST 0.5 eluted much more phage than Gly-HCl no matter what the elution order was. Since Gly-HCl disrupts the ionic bonds between phage and SWNTs while TBST 0.5 disrupts the hydrophobic interactions, we can conclude that the interaction between peptides and nanotubes is predominantly hydrophobic and thus TBST 0.5 is a better choice as an elution buffer for studying such interactions.

5.2.3. Wetting

While it is generally known that the surface of carbon nanotubes is hydrophobic, in our experiments this has given rise to some interesting observations not previously reported. In Figure 5.2 below, we show a photograph of two Si wafer samples of the same size: one containing only bare SiO_2, and the other coated with SWNTs. While the bare Si/SiO_2 sample sinks, the hydrophobicity of the SWNTs on the SWNT coated sample is sufficient to float the entire sample. More interestingly, when both of these samples were totally submerged in water, the SWNT sample can refloat to the surface by swirling the container several times while the bare SiO_2 wafer can not. This is a clear demonstration of the hydrophobicity of carbon nanotubes, even when on a SiO_2 surface. Measurements of water contact angles are consistent with this finding (data not shown). We use this finding later as a qualitative method to assay nanotube-phage interaction in various buffers.

Figure 5.2. A SWNT sample on a SiO2 wafer is suspended in water with the edge barely exposed to air while a SiO2 wafer with no nanotubes sinks to the bottom of the glass container before half of its area is submerged in the water.

5.2.4. CD measurements

CD spectra of peptide P1 was recorded for its aqueous solution and for a solution in TBS. The data indicates the peptide is a random coil, as shown in Figure 5.3 below.

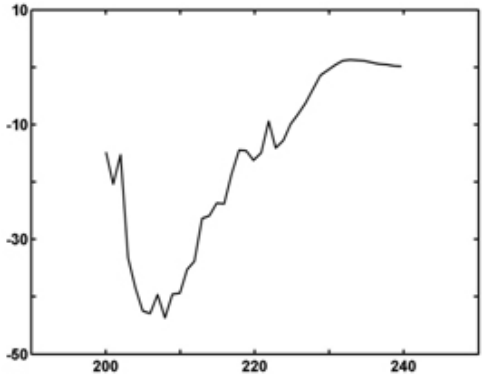

Figure 5.3. CD measurements of peptide P1.

5.2.5. Dispersion

A small amount of nanotubes were added to a 1% aqueous solution of peptide (P1) and the mixture was sonicated for several minutes. It was observed that even a prolonged sonication did not help in dispersing the nanotube in solution. This is in contrast to Dupont & Pender. This is evidence that our peptides are not surfactants.

5.2.6. Amino acid analysis

The percentage of each amino acid in the random library is known. We have compiled data of the relative occurrence of each amino acid in our peptides from the biopanning experiments, and the results are plotted in Figure 5.4.

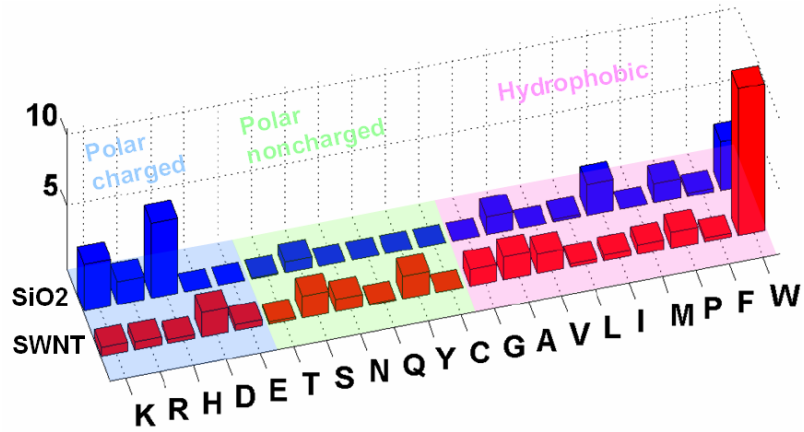

Figure 5.4. Relative occurrence of amino acids in nanotube and control experiments. The red and blue bars are for SWNT samples and their controls, respectively.

Histidine is a very commonly occurring amino acid in the control experiments. We interpret this as a binding sequence to SiO_2. The imidazole ring of histidine is protonated in aqueous solution while the SiO_2 surface is negatively charged. Hence the interaction between the peptides and SiO_2 is electrostatic. This electrostatic mechanism also explains the non-trivial occurrence of positive-charged lysine (K) shown in Figure 5.4.

In contrast, the W-rich peptides occur with high ratio only for the nanotube samples. Besides the peptides with the SXXWXXW motif, those W-rich peptides without showing the motif are believed to bind to SWNTs as well via the π-π interaction between the indole rings of Trp residues and the rings of SWNTs.

5.2.7. GES scale analysis

Using the GES scale[18], we have calculated the mean hydrophobicity for all the clones from each experiment. The results of this analysis are presented in Figure 5.5 below. It is clear that in the experiment where specific binders to SWNTs were found that the

peptides are the most hydrophobic. This is consistent with the known hydrophobicity of SWNTs and provides clues into the nature of the nanotube-peptide interaction. However, as shown in figure 5.6, in contrast to the DuPont work, our peptides are not symmetric surfactants, which we discuss next.

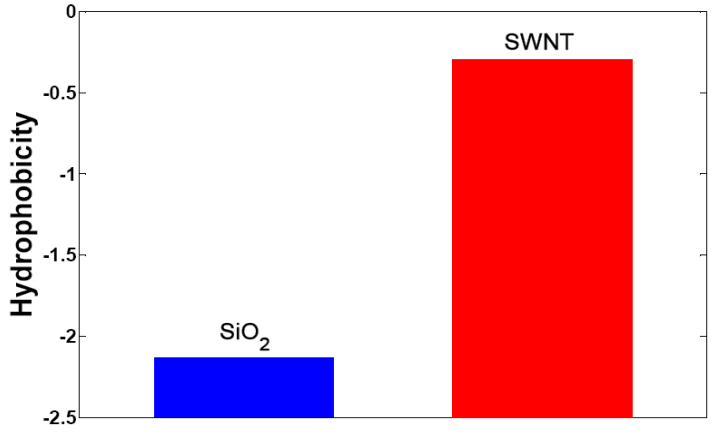

Figure 5.5. Mean hydrophobicity for nanotube and control binding peptides.

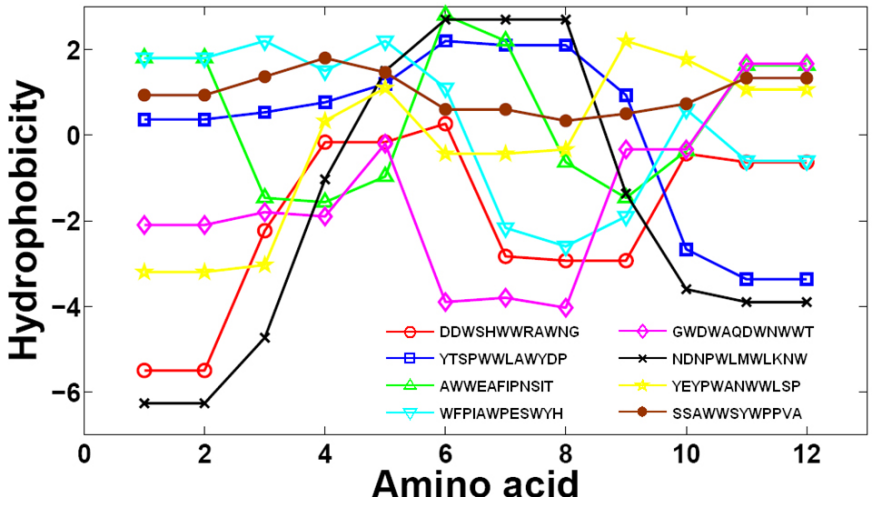

Figure 5.6. Amino acid hydrophobicity of nanotube-binding peptides using the GES scale.

5.2.8. Tryptophan location along motif

In Figure 5.7, we show helical wheel presentations of all the peptides bound to nanotubes. The results are striking. It is clear from this that the tryptophan residues are all located on one side of the helices. This general feature is included in all the sequences found that bind to SWNTs.

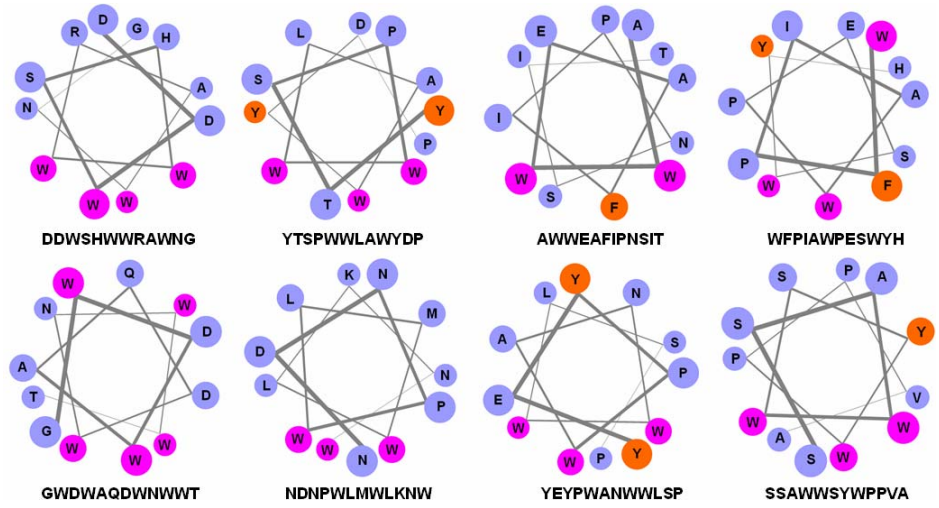

Figure 5.7: Helical wheel presentations of the peptides found which bind to SWNTs.

While the peptides were not shown to be alpha helices in the CD measurements, clearly there is some mechanism at play which tends to place Trp side groups along the sides of the helical wheel projection.

Also interestingly, in our motifs phenylalanine (Phe) hardly occurs at all. As Phe is a hydrophobic side group with aromatic content, it would reasonably be expected to occur in a nanotube binding motif. In fact, a nanotube binding peptide was also designed by Dieckmann et al[8] using predominantly Phe residues. It is not clear why our experiments

found predominantly Trp residues and not Phe also. Future experiments will aim to elucidate the relative binding affinity of CNT-Phe and CNT-Trp residues.

5.3. Conclusions

In our work we have found a tryptophan rich binding motif to SWNTs on a solid silicon substrate. Additionally, we found H-rich peptides which bind to the silicon substrate. Tryptophan seems to be very important in binding to CNTs, more so than F and Y. This is even true for non-surfactant binders, and for binding to CNTs on surfaces as well as in solution. While we have studied the binding to a heterogeneous mixture of (n,m) index SWNTs, we hope next to find binding motifs to nanotubes as a function of (n,m) index. This would involve the use of either one single long nanotubes[17], or the use of many identical tubes[19].

5.4. Experimental Section

5.4.1. Nanotube synthesis.

SWNT samples were prepared by densely growing SWNTs on thermal oxide passivated silicon wafers. Thermal oxide silicon wafers were obtained by oxidizing p-type silicon wafers with crystal orientation (100) at over 1000 ^{o}C to an oxide film thickness of about 1 μm. The silicon oxide wafers were then cut into 1 cm x 1 cm pieces with a dicing saw. After clean with acetone/methanol/DI water, some of quartz and silicon oxide wafers were reserved as control samples. The others were dipped into 1 mM $FeCl_3$ solution and rinsed with DI water followed by N_2 blow dry. These samples were then put into a 900 ^{o}C

furnace flowing methane and hydrogen to grow single-walled carbon nanotubes (see details [17] for growth methods). Representative SEM images of single walled carbon nanotubes on silicon wafers are shown in Figure 1A.

5.4.2. Phage display.

Phage display is a technique in which a random library of peptides is expressed on the surface of a phage virion[20]. The virions are allowed to incubate (bind) to a target (SWNTs in our case), while un-bound phage are washed away. The bound phage are eluted in a different buffer. The eluted phage contain sequences which bind to the target. To increase the specific selection, the cycle is typically repeated several rounds (9-10 rounds in our experiments), and then the phage DNA are sequenced to determine which peptide is expressed hence has binding affinity for the target. The overall procedure is indicated in Figure 1(B). In our experiments a random combinatorial library of 12-mer peptides (NEB Ph.D.-12 kit) expressed on the surface of M13 phage was used.

5.4.3. Titering and DNA sequencing.

The eluted phage with the *lacZα* gene are exposed to and thus infect the *E.Coli* ER2738 host strain (F'-recA^{+}*Δ(lacZ)*. The phage plaques appear blue when plated on LB/XGal/IPTG plates. The ratio of the total number of output phage after elution to the total number of input phage can be determined by titering the input and output eluate at each round (counting the numbers of blue plaques on plates). Blue plaques were randomly picked for DNA sequencing to detect the motif of the binding peptides.

5.4.4. Buffers.

There are four critical buffer solutions: blocking-buffer, incubation, wash, and elution buffers. Traditionally blocking buffers are used to prevent the binding of the exposed substrates. Incubation buffers allow binding to occur. Wash buffers remove unbound phage, while elution buffers eluate the bound phage for the next series of panning or sequencing. For traditional biological targets, a common blocking buffer solution is Bovine Serum Albumin (BSA); TBS containing 0.1% v/v Tween-20 (TBST 0.1) is typically used for the incubation buffer. The tween detergent is supposed to separate phage particles from binding to each other. The wash buffer is typically TBST 0.1 too for the first round and the tween concentration is increased stepwise by 0.1% the final concentration of 0.5%. Here tween prevents non-specific binding (NSB) to the target and the substrate. The elution buffer is typically glycine-HCl with pH around 2~3. We have varied these buffer solutions to obtain optimal results. Since SWNTs, which are very hydrophobic, were the targets in our experiments, these traditional buffers might not be all suitable. As expected, the results showed that one set of buffer solutions worked very well for carbon nanotube samples.

5.4.5 Peptide synthesis.

Peptides were synthesized using FMOC techniques by a commercial vendor ChemPep, Inc.and purified to 97.13%.

5.4.6 Dispersion experiments.

1 mg of SWNTs was added to 3 mL of 1% (w/v) peptide (P1) solution in DI water. The mixture was sonicated for 30 minutes and 1 hour. After the sonication mixture was centrifuged for 5 minutes.

5.5.7 CD measurements.

0.1 m molar solutions of peptide (P1) in DI water and TBS were prepared separately. CD measurements for these solutions were done using a 1mm quartz cell on a JASCO J-810 instrument. Spectra were recorded over the range of 180-260 nm with step size of 0.2 nm.

References

1. [Paul W. Barone, M. S. S., Reversible Control of Carbon Nanotube Aggregation for a Glucose Affinity Sensor. *Angewandte Chemie International Edition* **2006,** 45, (48), 8138-8141.
2. Yehia, H.; Draper, R.; Mikoryak, C.; Walker, E.; Bajaj, P.; Musselman, I.; Daigrepont, M.; Dieckmann, G.; Pantano, P., Single-walled carbon nanotube interactions with HeLa cells. *Journal of Nanobiotechnology* **2007,** 5, (1), 8.
3. Nadine Wong Shi Kam, Z. L. H. D., Carbon Nanotubes as Intracellular Transporters for Proteins and DNA: An Investigation of the Uptake Mechanism and Pathway. *Angewandte Chemie International Edition* **2006,** 45, (4), 577-581.
4. Moore, V. C.; Strano, M. S.; Haroz, E. H.; Hauge, R. H.; Smalley, R. E.; Schmidt, J.; Talmon, Y., Individually Suspended Single-Walled Carbon Nanotubes in Various Surfactants. *Nano Lett.* **2003,** 3, (10), 1379-1382.
5. O'Connell, M. J.; Bachilo, S. M.; Huffman, C. B.; Moore, V. C.; Strano, M. S.; Haroz, E. H.; Rialon, K. L.; Boul, P. J.; Noon, W. H.; Kittrell, C.; Ma, J.; Hauge, R. H.; Weisman, R. B.; Smalley, R. E., Band Gap Fluorescence from Individual Single-Walled Carbon Nanotubes. *Science* **2002,** 297, (5581), 593-596.
6. Zheng, M.; Jagota, A.; Semke, E. D.; Diner, B. A.; Mclean, R. S.; Lustig, S. R.; Richardson, R. E.; Tassi, N. G., DNA-assisted dispersion and separation of carbon nanotubes. *Nature Materials* **2003,** 2, (5), 338-342.
7. Zorbas, V.; Smith, A. L.; Xie, H.; Ortiz-Acevedo, A.; Dalton, A. B.; Dieckmann, G. R.; Draper, R. K.; Baughman, R. H.; Musselman, I. H., Importance of aromatic

content for peptide/single-walled carbon nanotube interactions. *Journal of the American Chemical Society* **2005,** 127, (35), 12323-12328.

8. Dieckmann, G. R.; Dalton, A. B.; Johnson, P. A.; Razal, J.; Chen, J.; Giordano, G. M.; Munoz, E.; Musselman, I. H.; Baughman, R. H.; Draper, R. K., Controlled assembly of carbon nanotubes by designed amphiphilic peptide helices. *Journal of the American Chemical Society* **2003,** 125, (7), 1770-1777.
9. Wang, S. Q.; Humphreys, E. S.; Chung, S. Y.; Delduco, D. F.; Lustig, S. R.; Wang, H.; Parker, K. N.; Rizzo, N. W.; Subramoney, S.; Chiang, Y. M.; Jagota, A., Peptides with selective affinity for carbon nanotubes. *Nature Materials* **2003,** 2, (3), 196-200.
10. Pender, M. J.; Sowards, L. A.; Hartgerink, J. D.; Stone, M. O.; Naik, R. R., Peptide-mediated formation of single-wall carbon nanotube composites. *Nano Letters* **2006,** 6, (1), 40-44.
11. Su, Z.; Leung, T.; Honek, J. F., Conformational Selectivity of Peptides for Single-Walled Carbon Nanotubes. *J. Phys. Chem. B* **2006,** 110, (47), 23623-23627.
12. Su, Z.; Mui, K.; Daub, E.; Leung, T.; Honek, J., Single-Walled Carbon Nanotube Binding Peptides: Probing Tryptophan's Importance by Unnatural Amino Acid Substitution. *J. Phys. Chem. B* **2007,** 111, (51), 14411-14417.
13. Hui Xie, E. J. B. R. H. B. A. B. D. G. R. D., Ranking the affinity of aromatic residues for carbon nanotubes by using designed surfactant peptides. *Journal of Peptide Science* **2008,** 14, (2), 139-151.
14. Poenitzsch, V. Z.; Winters, D. C.; Xie, H.; Dieckmann, G. R.; Dalton, A. B.; Musselman, I. H., Effect of Electron-Donating and Electron-Withdrawing Groups

on Peptide/Single-Walled Carbon Nanotube Interactions. *J. Am. Chem. Soc.* **2007,** 129, (47), 14724-14732.

15. Stanley Brown, T. S. Jespersen. J. Nygard., A Genetic Analysis of Carbon-Nanotube-Binding Proteins. *Small* **2008,** 4, (4), 416-420.
16. Yu, Z.; Li, S.; Burke, P. J., Synthesis of aligned arrays of millimeter long, straight single walled carbon nanotubes. *Chemistry of Materials* **2004,** 16, (18), 3414-3416.
17. Li, S. D.; Yu, Z.; Rutherglen, C.; Burke, P. J., Electrical properties of 0.4 cm long single-walled carbon nanotubes. *Nano Letters* **2004,** 4, (10), 2003-2007.
18. Engelman, D. M.; Steitz, T. A.; Goldman, A., Identifying Nonpolar Transbilayer Helices in Amino-Acid-Sequences of Membrane-Proteins. *Annual Review of Biophysics and Biophysical Chemistry* **1986,** 15, 321-353.
19. Arnold, M. S.; Green, A. A.; Hulvat, J. F.; Stupp, S. I.; Hersam, M. C., Sorting carbon nanotubes by electronic structure using density differentiation. *Nature Nanotechnology* **2006,** 1, (1), 60-65.
20. Baneyx, F.; Schwartz, D. T., Selection and analysis of solid-binding peptides. *Current Opinion in Biotechnology* **2007,** 18, (4), 312-317.

CHAPTER 6

CONCLUSION

In this thesis, we have described dielectrophoresis as an electronic analog of optical tweezers to manipulate particles and applied this technique to measure an upper limit on the conductance of DNA and protein molecules that were manipulated with DEP to bridge a gap between microfabricated electrodes. Based on this achievement, we demonstrated for the first time that carbon nanotubes, working as nanoelectrodes, can manipulate nanoparticles such as 20 nm polystyrene latex beads and 2 nm gold particles using the same technique. This purely electronic technique requires no mechanical motion at either the nano-scale or macro-scale. Thus, it is inherently scalable for massively parallel nano-manipulation. In addition, it should be possible to manipulate biological nanostructures using nanotube electrodes.

However, we do not know the type of bond that occurs at the attachment site. In order to investigate the interactions between carbon nanotubes and other materials, we have pursued phage display technique to determine amino acid sequences (peptides) which bind to single walled carbon nanotubes.

Based on our experimental results, we have found a tryptophan rich binding motif to SWNTs on a solid silicon substrate. Additionally, we found H-rich peptides which bind to the silicon substrate. Tryptophan seems to be very important in binding to CNTs, more so than F and Y. This is even true for non-surfactant binders, and for binding to CNTs on surfaces as well as in solution.

While we have studied the binding to a heterogeneous mixture of (n,m) index SWNTs, we aim eventually to demonstrate such a method in nanotubes of a specific (n,m) index, and to develop a bio-mimetic toolbox for non-covalent nanotube manipulation. Such a toolbox will aid in the manipulation, and, eventually, enzymatic synthesis, of carbon nanotubes.

APPENDIX

A-1 Media and solutions

LB Medium (per liter):

10 g Bacto-Tryptone, 5 g yeast extract, 5 g NaCl. Autoclave, store at room temperature.

LB/IPTG/Xgal Plates:

LB medium + 15 g/L agar. Autoclave, cool to < 70°C, add 1 ml IPTG/Xgal* and pour. Store plates at 4°C in the dark.

Agarose Top (per liter):

10 g Bacto-Tryptone, 5 g yeast extract, 5 g NaCl, 1 g $MgCl_2 \cdot 6H_2O$, 7 g agarose. Autoclave, dispense into 50 ml aliquots. Store solid at room temperature, melt in microwave as needed.

Tetracycline Stock:

20 mg/ml in Ethanol. Store at –20°C in the dark. Vortex before using.

LB-Tet Plates:

LB medium + 15 g/l Agar. Autoclave, cool to <70°C, add 1 ml Tetracycline stock and pour. Store plates at 4°C in the dark. Do not use plates if brown or black.

Blocking buffer:

0.1 M $NaHCO_3$ (pH 8.6), 5 mg/ml BSA, 0.02% NaN_3. Filter sterilize, store at 4°C.

PEG/NaCl:

20% (w/v) polyethylene glycol–8000, 2.5 M NaCl. Autoclave, store at room temperature.

TBS:

50 mM Tris-HCl (pH 7.5), 150 mM NaCl. Autoclave, store at room temperature.

Iodide Buffer:

10 mM Tris-HCl (pH 8.0), 1 mM EDTA, 4 M NaI. Store at room temperature in the dark.

Streptavidin Stock Solution:

Dissolve 1.5 mg Lyophilized Streptavidin (supplied) in 1 ml 10 mM sodium phosphate (pH 7.2), 100 mM NaCI, 0.02% NaN3. Store at 4°C or –20°C (avoid repeated freezing/thawing).

**Note for IPTG/Xgal: Mix 1.25 g IPTG (isopropyl β-D-thiogalactoside) and 1 g Xgal (5-Bromo-4-chloro-3-indolyl-β-D-galactoside) in 25 ml Dimethyl formamide. Solution can be stored at –20°C in the dark.*

A-2 Protocol of phage display for the SWNTs on chips and the control samples

Day 1

1 Inoculate 10 ml LB medium with ER2738 for tittering. Incubate the culture at 37°C with vigorous shaking until OD600 = 0.5 (mid-log phase).

2 Inoculate 25 ml LB medium with ER2738 for samples in a 250 ml Erlenmeyer flask. Incubate both cultures at 37°C with vigorous shaking until OD600 ~ 0.05-0.1 (early-log phase).

3 Mix 1 ml of TBS and 10 μl phage (4×10^{10}) from the NEB phage library in a well of a culture plate. Immerse the SWNT wafer in the phage solution. Rock gently, 45 minutes @ RT. Do the same to its control sample (the sentence is not repeated below).

4 Take out the SWNT wafer and wash it 5X, each time in a new well with 1 ml TBS.

5 Add 1 ml TBST 0.5 to a new well. Put the SWNT wafer into the well and rock gently for 45 minutes.

6 Take out the SWNT wafer and put it into a new well of a new plate and rinse with ddH2O 5 times. Pipet the eluate into a new microtube and label it.

7 Titer a small amount (~ 10 μl) of the eluate. Follow the phage titering procedure. Usually 100X, 1000X, 10^4X and 10^5X for the unamplified eluate.

8 Add the rest of the eluate to the 10 ml early-log ER2738 culture in step 2. Incubate / vigorously shake @ 37°C, 4.5 hours.

9 Pipet the culture into 8 microtubes, 1.25 ml each (only microcentrifuge is available in our lab). Spin 10 minutes @ 16,000 rpm / 4°C. Transfer the supernatant to new microtubes and re-spin.

10 Pipet the upper 80% of the supernatant to the new microtubes and add 1/6 volume of PEG/NaCl. Allow phage to precipitate at 4°C overnight

Day 2

11 Do step 1 and 2. Count and record the blue plaques for the unamplified eluate.

12 Spin 8 microtubes of PEG precipitation, 15 minutes @ 16,000 rpm / 4°C. Decant supernatant, re-spin briefly, and remove residual supernatant with a pipette.

13 Suspend the pellets together in 1 ml TBS. *(Here is how for 8 microtubes: suspend pellets of 4 of tubes each with 250 µl TBS*; *transfer 250 µl in the 4 tubes into another 4 tubes; mix the solution in the last tube.)*

14 Spin for 5 minutes at 4°C to pellet residual cells.

15 Transfer the supernatant to a new microtube. Re-precipitate with 1/6 volume of PEG/NaCl. Incubate on ice 45 minutes. Spin 10 minutes @ 4^{o}C. Discard supernatant, re-spin briefly, and remove residual supernatant with a micropipet.

16 Suspend the pellet in 200 µl TBS, 0.02% NaN3. Spin 1 minute to pellet any remaining insoluble matter. Transfer the supernatant to a new tube (*Note: This is the amplified eluate).* Label it.

17 Titer a small amount (~ 10 µl) of the eluate. Follow the phage titering procedure. Usually 10^{6}X, 10^{7}X, 10^{8}X and 10^{9}X for the unamplified eluate, depending on the

titering results of the unamplified eluate. Count and record the blue plaques for the amplified eluate.

18 Estimate the volume of the amplified eluate for 10^{10} phages. It might need 100-150 μl for the second round of panning. But the volume should be less for the subsequent rounds since more specific-binding phages are amplified.

19 Mix that much volume of the amplified eluate with 1 ml TBS in a well of a new culture plate. Put the same SWNT sample into the well and rock gently for 45 minutes @ RT.

20 Do steps 4-10.

Day 3, 4, 5, …

21 Do steps 11-20 until the motif of the sequences is achieved.

The general procedure is show in Figure A-2.1.

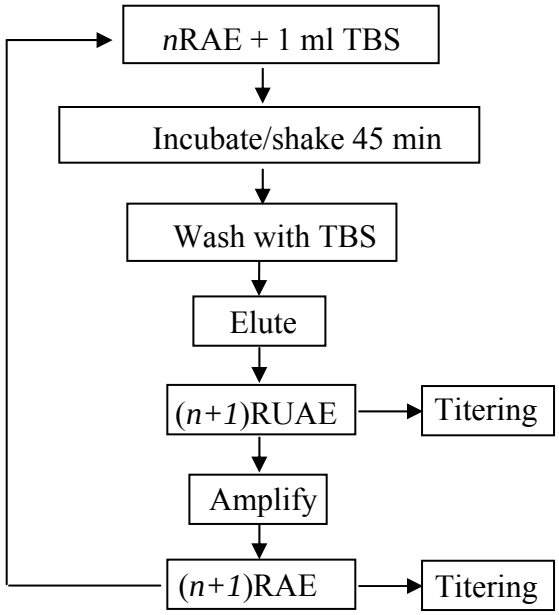

Figure A-2.1. The schematic process for phage display experiments. RT stands for Room Temperature; *n*R(U)AE for the *n*th-Round of (Un)Amplified Elution. 10 μl NEB phage is used for 0RAE.

A-3 Protocol of phage titering

1 Inoculate 5–10 ml of LB with ER2738; incubate with shaking until OD_{600} ~ 0.5.

2 Melt Agarose Top in microwave and dispense 3 ml into sterile culture tubes, one per expected phage dilution. Equilibrate tubes at 45°C.

3 Pre-warm 1 LB/IPTG/Xgal plate per expected dilution at 37°C.

4 Prepare 10-fold serial dilutions of phage in LB.

5 Dispense 200 µl mid-log culture into microtubes, 1 for each phage dilution.

6 Add 10 µl of each dilution to each tube, vortex quickly, and incubate at room temperature for 1–5 minutes.

7 Transfer the infected culture to a culture tube containing 45°C Agarose Top, vortex quickly, and pour onto a LB/IPTG/Xgal plate. Swirling the plate to spread Agarose Top evenly.

8 Allow plates to cool 5 minutes, invert and incubate overnight at 37°C.

9 Inspect plates and count plaques on plates having ~100 plaques.

An example of a note sheet for titering is shown in table A-3.1

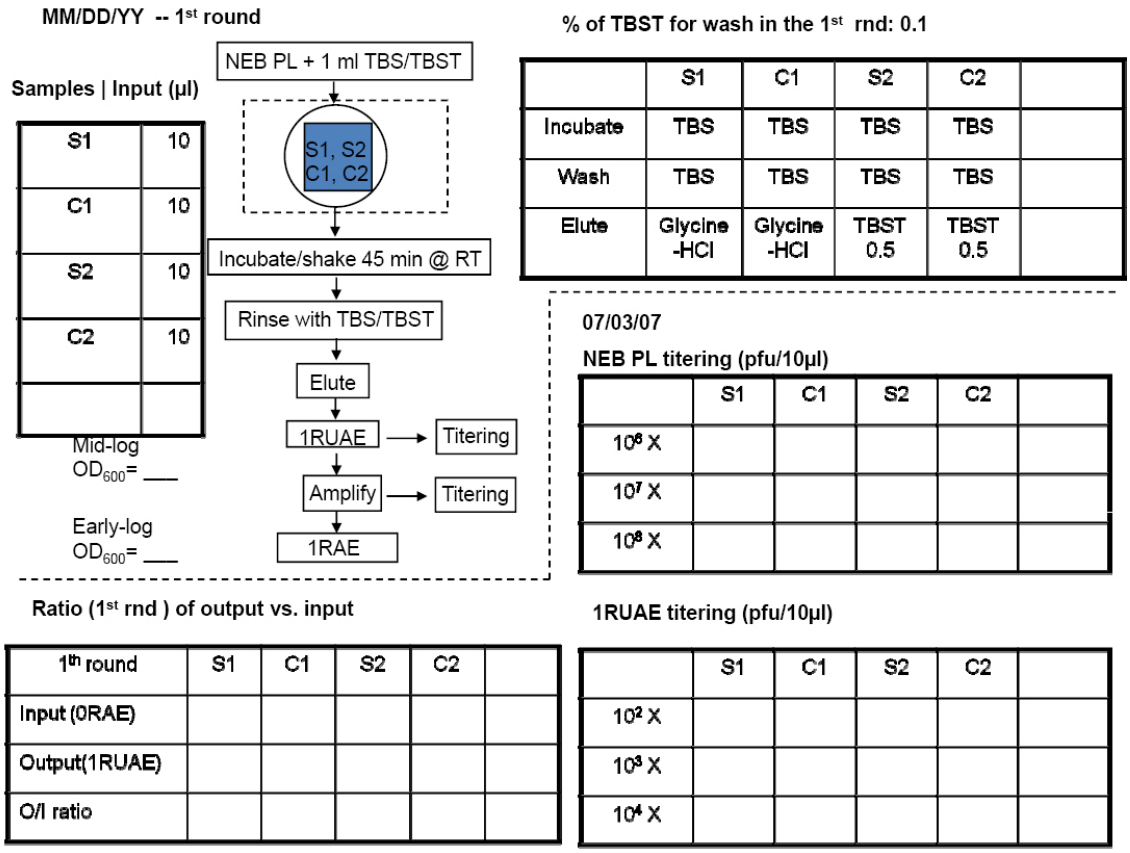

Table A-3.1 Example of the tetering note sheet

A-4 Protocol of characterization of binding clones

1 Culture the ER2738 overnight (~ 14 hours) in a 250 ml Erlenmeyer flask and dilute 1:100 in LB. Dispense 1 ml diluted culture into each of 10 culture tubes.

2 Stab 10 blue plaques each with a new pipet tip and transfer them to the 10 culture tubes of step 1.

3 Incubate tubes at 37°C with shaking for 4.5 hours.

4 Transfer cultures to microcentrifuge tubes, centrifuge 30 seconds. Transfer 500 µl of the supernatant to a new microcentrifuge tube.

5 Add 200 µl PEG/NaCl. Invert to mix, stand 10 minutes @ RT.

6 Centrifuge 10 minutes, discard supernatant. Re-spin briefly. Carefully pipet away any remaining supernatant.

7 Suspend pellet thoroughly in 100 µl Iodide Buffer and add 250 µl ethanol.

8 Incubate 10 minutes @ RT.

9 Spin 10 minutes, discard supernatant. Wash pellet in 70% ethanol, dry briefly under vacuum.

10 Suspend pellet in 30 µl TE buffer.

11 Measure the density of ssDNA (ng/µl). Calculate the volume for 500 ng ssDNA.

12 Calculate the difference of 8 ml and the volume of ssDNA for ddH2O. Set 8 ml ssDNA and 0 for H2O if the volume of ssDNA is over 8 ml.

13 Mix the ssDNA and ddH2O in PCR strips.

14 Mail the PCR strips to Genewiz for sequencing.